Distribution Agreement

In presenting this thesis as a partial fulfillment of the requirements for a degree from Emory University, I hereby grant to Emory University and its agents the non-exclusive license to archive, make accessible, and display my thesis in whole or in part in all forms of media, now or hereafter now, including display on the World Wide Web. I understand that I may select some access restrictions as part of the online submission of this thesis. I retain all ownership rights to the copyright of the thesis. I also retain the right to use in future works (such as articles or books) all or part of this thesis.

Kelly M. Jones   April 11th, 2019

Developing Methods Towards Quantifying and Enhancing the Endosomal Escape of DNA-Gold
Nanoparticle Conjugates

by

Kelly M. Jones

Dr. Khalid Salaita Ph.D.
Adviser

Department of Chemistry

Dr. Khalid Salaita Ph. D.

Adviser

Dr. Stefan Lutz Ph.D.

Committee Member

Dr. Cherry Wongtrakool M.D.

Committee Member

2019

Developing Methods Towards Quantifying and Enhancing the Endosomal Escape of DNA-Gold
Nanoparticle Conjugates

By

Kelly M. Jones

Dr. Khalid Salaita Ph.D.

Adviser

An abstract of
a thesis submitted to the Faculty of Emory College of Arts and Sciences
of Emory University in partial fulfillment
of the requirements of the degree of
Bachelor of Sciences with Honors

Department of Chemistry

2019

Abstract

Developing Methods Towards Quantifying and Enhancing the Endosomal Escape of DNA-Gold
Nanoparticle Conjugates
By Kelly M. Jones

This thesis is divided into five chapters. The first chapter provides background for development of spherical nucleic acids (SNAs) and focuses on a particular type: DNA-gold nanoparticle (DNA-AuNP) conjugates. The introduction provides detail into the design, commercial availability, therapeutic applications, and intracellular uptake of DNA-AuNPs. It includes a brief summary of our contribution to the field via the development of deoxyribozyme-gold nanoparticle (Dz-AuNP) conjugates. Additionally, the introduction discusses an ongoing debate as to whether DNA-AuNPs, as well as other SNAs, achieve significant cytosolic access or primarily remain sequestered in endosomes. The second chapter describes work to develop a method to quantify and assess the intracellular location of these particles through a split green fluorescent protein (GFP) complementation assay. In our hands, the assay proved to be insensitive for the desired intracellular applications. The third chapter describes the ongoing investigations of a ratiometric assay that utilizes two fluorescent dyes, fluorescein (FAM) and ATTO647N, to develop a standard curve of their pH-dependent fluorescence intensity ratio. This chapter contains extensive findings of the in-development assay with the goal of determining the intracellular and environmental pH of these probes. The fourth chapter describes work toward the synthesis and characterization of known endosomal enhancing peptides. Chapter 4, also, discusses the potential effects of conjugating endosomal disrupting peptides to pH-sensing AuNPs. Finally, Chapter 5 contains an overall discussion and conclusion of this thesis. Future directions for this project and the implications our findings are detailed here.

Developing Methods Towards Quantifying and Enhancing the Endosomal Escape of DNA-Gold
Nanoparticle Conjugates

By

Kelly M. Jones

Dr. Khalid Salaita Ph.D.

Adviser

A thesis submitted to the Faculty of Emory College of Arts and Sciences
of Emory University in partial fulfillment
of the requirements of the degree of
Bachelor of Sciences with Honors

Department of Chemistry

2019

Table of Contents

Table of Figures

Chapter 1: Introduction

Figure 1.1. Left shows a single-stranded DNA-gold nanoparticle conjugate (adapted from Mirkin Group). Right shows schematic for DNA-gold nanoparticle synthesis.

1. Introduction

1.1. Nanomaterials as Therapeutics

Within the last twenty-five years, the fields of medicine and dentistry have evolved in the wake of staggering advancements in nanotechnology and nanomaterial science. Nano-sciences pertain to molecular and nanometer scale developments in fields like chemistry, biology, and physics.[1] Nanomedicine, a promising and emergent field, utilizes technologies designed at these minute scales and applies them to living systems as a means of drug delivery, screening technology, gene therapy, and tissue engineering.[2-5] One challenge faced in nanotechnology is the ability to reproducibly create uniform nanostructures, but this can be overcome in chemical and biological platforms using bottom-up "self-assembly" manufacturing. Self-assembly relies on known characteristics of macromolecules, like DNA's affinity to hybridize with a complementary strand, to predictably assemble complex structures.[2] Often these characteristics are simply intra- and intermolecular effects inherent in many biological molecules, but their implications in developing nanotechnologies can be far reaching. In this chapter, we describe a family of nanotechnologies which utilizes self-assembly and delve into the characterization and enhancement of their intracellular trafficking.

1.2. DNA-Gold Nanoparticle Conjugates

The first reports of DNA-gold nanoparticle conjugates were two communication letters to *Nature*. They were published in 1996 and discussed the coincidentally concurrent development of reversibly self-assembling, colloidal gold nanoparticle aggregates.[6, 7] In the first article, two batches of 13 nm gold nanoparticles (AuNPs) were functionalized with thiolated single-stranded DNA (ssDNA), of known and noncomplementary sequences.[6] These DNA-functionalized AuNPs are now known as DNA-gold nanoparticle (DNA-AuNP) conjugates. Upon addition of a "sticky ended" DNA duplex, with each end a complement of the functionalized sequences, the two batches of DNA-AuNP conjugates self-assembled into aggregates that could be thermally denatured.[6] The second article, ironically published on the following page of the same *Nature* issue, similarly discusses the novelty of functionalizing ssDNA to gold nanostructures and the self-assembling organization arising from duplex hybridization.[7] After their initial publications, Mirkin, Alivisatos, and others have since published many papers further developing, delineating, and applying this nanomaterial. DNA-AuNP structures now comprise a small portion of a much larger family of DNA-linked nanomaterials, known as spherical nucleic acids (SNAs).[8]
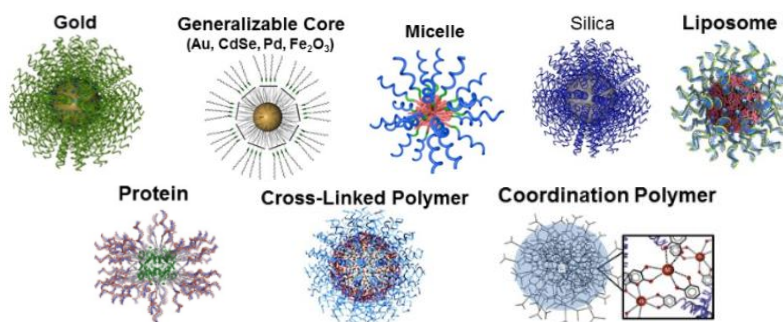
Figure 1.2. Image of the extensive family of nanomaterials that are characterized under the term spherical nucleic acids (SNAs) (adapted from Mirkin Group).

The term SNA not only includes ssDNA-AuNP constructs, but as seen in **Figure 1.2.**, includes variation in: the type of oligonucleotides conjugated (single-/double-stranded RNA or single-/double-stranded DNA); the core identity (silica, silver, lipid, and coreless varieties); and even the core shape (nano-rods, -prism, etc.).[8] Although each subtype may have differences in their application and character, what relates each is the shared stabilizing electrostatic and repulsive effects. These effects arise as a result of the dense shell of oligonucleotides conjugated in their three-dimensional architecture. The shell provides shielding of the oligonucleotides from degradation by nucleases which otherwise cripples soluble oligonucleotides, when delivered to cells.[9] In addition to nuclease protection, SNAs trigger reduced immune response compared to that of their soluble counterpart.[8] Again, this arrangement provides superior protection for sequences exposed to cells. Another difference between SNAs and soluble nucleic acids is that the spherical construct of SNAs are readily up-taken by cells.[8, 9] Indeed, virtually all nucleated cells uptake SNAs.[10] In stark contrast, soluble oligonucleotides experience minimal intracellular delivery. In fact, their delivery is inefficient and often requires cationic transfection agents *in vitro*.[8, 11]

1.3. Commercially Available and Clinically in-Development SNAs

SNAs are currently on the market as novel forms of intracellular probes. Nano-Flares, with the commercial name of SmartFlares, is one such example. Nano-Flares are probes designed to detect specific intracellular mRNA transcript sequences. The probes are functionalized with a single-stranded oligonucleotide sequence, or "recognition sequence", that can complement with both the target mRNA transcript and what is known as a "reporter sequence". The reporter sequences are shorter sequences, labeled with a fluorescent dye that is quenched when the

sequence is complemented to the probes. The quenching is a result of the gold nanoparticles core's absorption spectrum overlapping with the emission spectrum of the dye. Upon cellular entry, the reporter sequence is displaced (due to its lower melting temperature) from the recognition sequence by the hybridization of the target mRNA transcript. Release of the reporter sequence then results in an increase in the dye's fluorescence intensity because the nanoparticle is no longer close enough to execute quenching.[5, 12, 13] These probes have the capacity to target any mRNA transcript because the recognition and reporter sequences can be accordingly varied.[13] The live cell application of these probes to detect specific mRNA levels is a highly sought-after tool.

Additionally, several forms of SNAs for gene regulation are currently under investigation. One such SNA includes an RNA-based AuNP conjugate that is currently in Phase 1 clinical trials for treating recurrent glioblastoma multiforme (GBM) patients.[14] The drug relies on RNA interference (RNAi) to downregulate oncogene expression.[4] Briefly, RNAi therapy generally works by its complementation with an mRNA transcript, resulting in transcript degradation.[15] The therapy showed enhanced intracellular delivery capabilities, as compared to soluble RNAi therapies, without the need of auxiliary transfection agents or modification. A major issue of targeting GBM is not only the inability of RNAi therapies to successfully enter cells, but also to permeate the blood-brain barrier.[4] Both of these constraints appear to be overcome by this SNA therapy in pre-clinical trials and its efficacy is still being studied.

Another form of SNA that has shown promising therapeutic results, includes a fatty acid core functionalized with DNA or modified DNA that has been used in human trials to combat psoriasis.[16, 17] This drug reportedly works via antisense (AS) gene regulating mechanisms, similar

to those of asDNA-AuNP conjugates. Instead, this therapy relies on modified oligonucleotides functionalized to a fatty acid core NP.[18] Gene silencing through antisense DNA is a method of trapping mRNA transcripts to prevent their translation (or, expression) by ribosomes and/or relies on RNase H activity to cleave the transcript.[19] In the latter method, RNase H selectively cleaves DNA-RNA duplexes.[16, 19] Because antisense therapies are typically reliant on soluble oligonucleotides, historically, they have faced difficulty with intracellular delivery and nuclease degradation.[20] By conjugating these sequences in an SNA conformation, this obstacle is overcome which makes this approach an encouraging gene regulation technique.
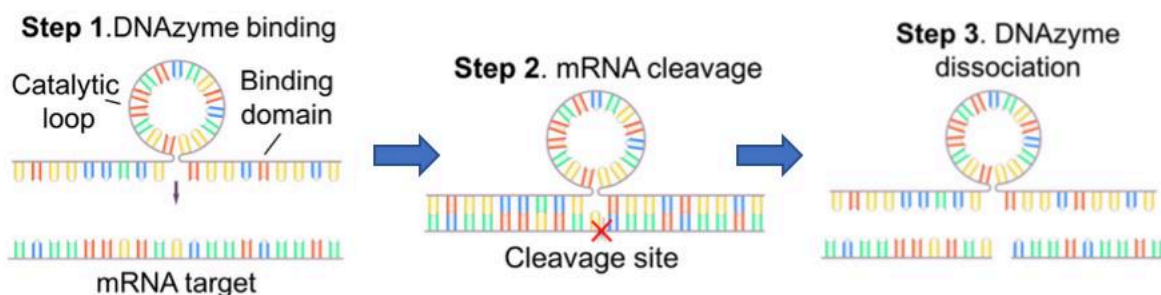
Figure 1.3. Catalytic action of DNA enzymes on target mRNA transcript. Following Step 3, the DNAzyme is free to repeat the process by hybridizing with a new mRNA target.

1.4. DNAzyme-AuNP Conjugates

Deoxyribozymes, or DNAzymes, are synthetic single-stranded oligonucleotide sequences capable of catalyzing and/or performing chemical reactions with high selectivity and significant efficiency.[21, 22] These enzymatic-like capabilities have enabled DNAzymes (Dz) to participate in various biological roles, including aiding in understanding gene function and use as therapies.[23] Their ability to act as gene regulation agents is attributed to innate catalytic mechanisms dependent on the divalent cation sequestered in their catalytic loop. Upon hybridization of the DNAzyme with its complementing mRNA transcript, the transcript is cleaved, and the result is

transient gene silencing.[21, 22] The conjugation of DNAzymes to gold nanoparticles has become a topic of major interest by the Salaita Group and their potential therapeutic implications are wide-ranging.[10, 23, 24]

In 2012, Yehl et al. published a paper regarding overcoming the difficulties associated with cellular uptake of catalytically active oligonucleotides, specifically DNAzymes.[23] Because of the inherent stability and uptake enhancing characteristics of DNA functionalized gold nanoparticles, adaptation of this technology for catalytically active DNAzymes arose to show that Dz-AuNPs can readily enter cells to preform gene regulation.[23] That paper functioned as a steppingstone for future DNAzyme-based gold nanoparticle technologies.[10, 24] This construct was used to knockdown expression of tumor necrosis factor-α (TNF-α), a pro-inflammatory cytokine.[10] The Dz-AuNP constructs were applied to act as an anti-inflammatory to treat myocardial infarction in rodent models.[10] Most recently, Petree et al. published a paper showing a spliceosome-mimicking DNAzyme-AuNP conjugate functionalized with three different enzymes. Two of the enzymes are DNAzymes and the third an RNA ligase.[24] The Dz-AuNP acts by doubly-cleaving an mRNA transcript and ligating the two external sequences. The inherent variability of DNAzyme sequences and of AuNP architectural design provides exciting opportunities to target a wide range of genes.

1.5. Endocytosis and Fate of DNA-AuNP Conjugates

The semipermeable nature of a cell membrane limits the character of bioactive materials capable of gaining entry. Materials with large size, hydrophilic components, or significant charge often experience difficulty while attempting to cross the phospholipid bilayer. Receptor mediated endocytosis is one method of entry for materials that do not have transport protein

mediated transmembrane delivery vehicles.[25, 26] Because endocytosis results in external material uptake and confinement within an endosome (with a semipermeable membrane of its own), the same difficulties with crossing a lipid membrane are present. And thus, through endocytosis, entry into the cytosolic compartment is further constrained by endosomal trafficking.[27]

The life of an endosome and its contents are varied. The endosome can reunite with the plasma membrane to release the recently endocytosed material and recycle its receptors; cargo can be sent to the trans-Golgi network; or the contents can be slated for degradation.[27, 28] If the latter, the endosomes mature from early endosomes to late endosomes and this maturation is accompanied by an increase in their acidity.[27] An early endosome is characterized by a pH of ~6.5; while a late endosome is characterized by a pH of ~5.5.[27] The influx of protons continues to lower the pH of late endosomes and, thus, they mature into lysosomes with a pH of ~4-5.[28] The highly acidic environment of lysosomes and late endosomes contain enzymes and redox active species, all of which aid in the breakdown of various metabolites.[27, 28]

It has been established that the spherical architecture of DNA-AuNP conjugates aids in their cellular uptake.[8] They do not require transfection agents and are believed to engage in receptor mediated endocytosis.[8, 29, 30] Although mechanisms of uptake are not universally established, colocalization studies have found that after 1-2 hours of incubation, they reside in early endosomes.[30] From 4-24 hours, particles are determined to be within late endosomes. At about 16-hours after uptake, the oligonucleotides are stripped from the gold core by nucleases within late endosomes and these fragments are recycled out of the cell.[30] Interestingly, within the 24-hour window, DNA-AuNP conjugates do not enter lysosomes nor are they transported to the trans-Golgi network—which is typical of most biological material degradation pathways. Rather,

in late endosomes clustering of particles occurs. These clusters indicate that the oligonucleotides once conjugated to the cores have been degraded.[30]

After endocytosis, the intracellular fate of DNA-AuNP conjugates has proved to be a point of contention. Despite endosomal entrapment, "a small, unquantifiable portion of DNA-AuNP conjugates escape the endosome and are found in the cytosol;" the portion that escapes is responsible for any gene regulation these nanomaterials are known to exhibit.[5] Admittedly, this explanation of endosomal escape seems fairly vague and has received backlash from several groups.[31-34] These groups question whether DNA-AuNP conjugates are capable of their advertised ability to escape the endosomes and act as sensing and imaging reporters of intracellular events. It even brings into question whether the DNA-AuNP conjugates achieve escape at all.

One such opponent, Raphaël Lévy, has self-published several pieces that argue DNA-AuNP conjugates do not escape endosomes.[31-33] Instead, he argues the DNA-AuNPs are degraded within endosomes and any increasing fluorescence ("misinterpreted" as activity) actually arises from the disassociated fluorescent oligonucleotides that are no longer quenched by the gold particle.[31] He severely attacks the vague explanations of escape reported by Mirkin, Merck Millipore, and others. His primary qualm with their ambiguity is founded upon the historic uses of gold nanoparticles. AuNPs have been used extensively to study intracellular trafficking and, therefore, he believes it should not be difficult to study the trafficking of gold nanoparticles functionalized by DNA.[32, 33] In a somewhat impudent, but possibly fair assertion, Lévy suggests one reason Mirkin's papers have been published (and Lévy's require self-publishing) is because

of Mirkin's prominence in the nanotechnology field and his relationship with various journals.[33]

Lévy suggests that further investigation be done to confirm the mechanism of escape.[32]

Despite Lévy's crusade, a more recent report was published validating his claims that SmartFlares do not report on their target mRNA transcripts.[34] Titled "SmartFlares fail to reflect their target transcript levels," the report cites Lévy's self-published work and elaborates on the shortcomings of this technology. The paper reports the fluorescence intensities of five different SmartFlare probes to be independent of their target mRNA levels (as measured by RT-qPCR). The probes also "failed to distinguish" between target mRNA-expressing and non-expressing cell lines. Finally, the paper provides evidence that suggests SmartFlare fluorescence intensity is a function of the cell's ability to internalize and retain the probes.[34] The paper does suggest that SmartFlares do not appear to be degraded in lysosomes and offers its methods in an attempt to provide others with guidelines for better controls to minimize data misinterpretation.

In an effort to clarify the intracellular trafficking of nucleic acid conjugated-AuNPs, a recent paper was published describing the development of a pH-sensitive ratiometric dsDNA-AuNP probe (called the pH-BOT).[35] Various pH-sensitive probes have been developed for other nanotherapeutic designs; however, there had yet to be reported one that monitors intracellular delivery of gold core nanoparticles.[35-38] Their findings agree that SNAs are endocytosed within one-hour of transfection.[30, 35] However, they report the DNA cargo is released from the AuNPs with a half-life of 1.5-hours. The Strouse et al. paper does agree that DNA constituents remain in late endosomes for up to 24-hours.[30, 35] The slow in DNA degradation, previously attributed to SNA shape (by Mirkin and others) is, by this paper, believed to be a result of pH buffering. The buffering is described to arise from the protonation of the thiol group ($pK_a > 10$) previously used

as a linker for the DNA to the AuNP. This pH buffering purportedly accounts for the slow in endosomal maturation and acidification.[35] These results should be considered with the caveat that the particles were 6.6 nm in diameter, slightly smaller than other SNA constructs. Additionally, they were modified with dsDNA, which may alter endosomal dynamics compared to that of ssDNA-AuNP conjugates. A third consideration is the presence of three organic dyes which could similarly alter behavior. The pH-BOT work shares some of the goals outlined in this thesis and will be discussed at greater length in Chapter 3.

1.6. Overview of Goals

The overall goal of this thesis is to develop a new tool that can address the controversy in the field pertaining to the endosomal escape of DNA-gold nanoparticle conjugates. By developing a probe that can report on the endosomal trafficking and escape of 13 nm ssDNA-AuNP conjugates, we will be able to determine when and whether our DNA-AuNP conjugates successfully escape the endosome. This will help corroborate other investigations and provide insights into the mechanism of DNA-AuNP activity. Chapters 2 and 3 will address past and ongoing attempts to develop such a probe. Chapter 4 will address the screening of known endosomal escape enhancing peptides and amino acid domains. We are hoping that these sequences demonstrate their known function of rupturing endosomal bilayers while maintaining the integrity of the cell's membrane. And finally, Chapter 5 will summarize this work and detail future steps for this project.

Chapter 2: Quantifying Endosomal Escape Using a Split GFP Complementation Assay

Author Contributions

K.M.J. and B.R.D. designed this project, performed these experiments, and analyzed this data. All contributors discussed results and gave input.

2. Quantifying Endosomal Escape Using a Spilt GFP Complementation Assay

2.1. Background and Design

The green fluorescent protein (GFP), is aptly named for its green fluorescent quality when irradiated with 480 nm light. It is a three-dimensional β-barrel protein composed of eleven β-strands. [39] The 238 amino acid length sequence has a molecular mass of 27 kDa, a diameter of 2.4 nm, and cylindrical length of 4.2 nm. [40, 41] With an emission wavelength in the visible spectrum (~510 nm), it has extensive intracellular applications.[39, 40]
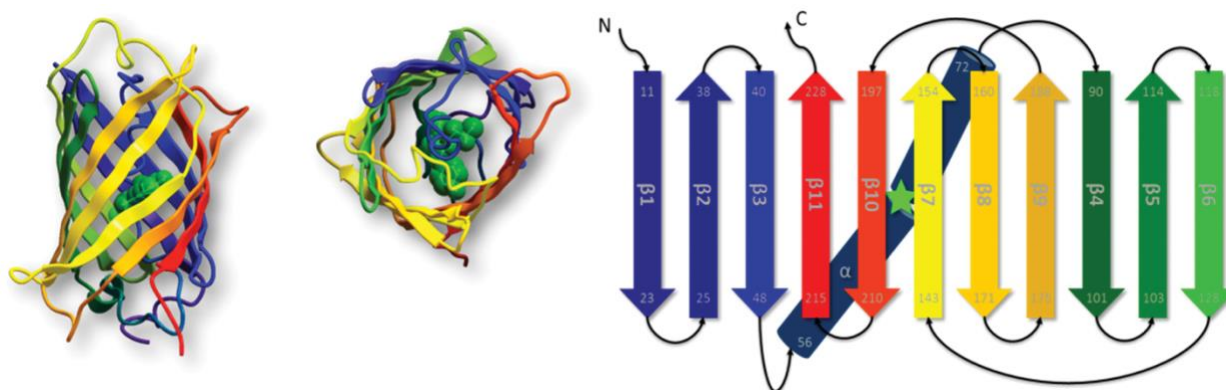
Figure 2.1. A three-dimensional structure of the green fluorescent protein as determined by x-ray crystallography. The first two images show the fully folded protein from a side-on and over-head view, respectively. The third image shows the unfolded, antiparallel β-strands with their respective numbers and the internal chromophore structure is indicated by the star. Adapted from GFP-Based Biosensors.[42]

Like many other proteins, GFP can be cleaved into two separate and stable components, GFPβ1-10 and GFPβ11, which will reassemble noncovalently and irreversibly through intermolecular, hydrophobic and electrostatic interactions, or protein-protein interactions (PPI).[39, 43-45] GFPβ1-10 mostly maintains its β-barrel structure despite the missing 11th strand and this retention of shape allows for easy reassembly. The GFPβ1-10 structure contains the three amino acid residues that compose its chromophore (Ser65, Tyr66, and Gly67), but with 11th strand absent, they are not in close-enough proximity to cyclize. This is why, unlike complete GFP,

the separated sequences should not exhibit fluorescence when excited with light. Upon complementation, the fluorescent character is restored and is indistinguishable from unmodified GFP.[39]

This complementation phenomenon has been applied to various biological systems and, more importantly, the recombination process has been used to test the efficacy of various nanotechnologies.[40, 46-49] Historically, split GFP complementation assays have been used to determine whether two proteins associate. One protein is tagged with GFPβ11, while the protein's potential partner is tagged with GFPβ1-10. Upon protein binding, the full GFP forms, thus leading to fluorescence.[46, 47] More recently, an adapted assay has been developed to test for endosomal escape.[48-50] Here we attempted to similarly apply a split GFP complementation assay to screen the location of our DNA-gold nanoparticle conjugates incubated in cells in order to test whether escape does in fact occur.
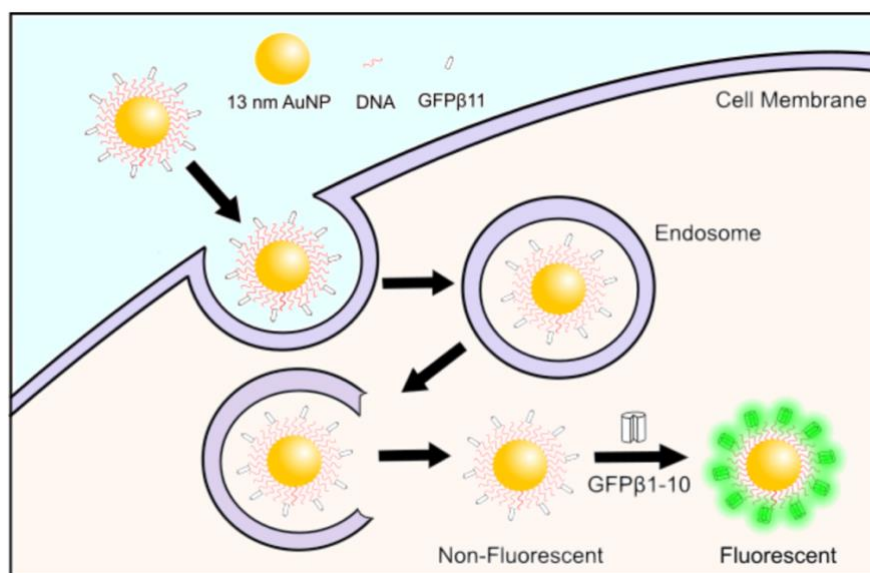
Figure 2.2. Schematic diagram illustrating the fluorescence arising from assembly of GFPβ11-T20-DNA-AuNP with GFPβ1-10 upon the AuNP's access to cytosolic compartment of a cell.

The design of our assay, as illustrated in **Figure 2.2.**, requires GFPβ1-10 to be expressed in cells by plasmid transfection. Synthetic GFPβ11 is conjugated to 3'-thiolated ssDNA through either: biotin/streptavidin interactions or covalently through NHS-azide chemistry. The 3' terminus of this DNA-peptide construct is then functionalized to 13 nm gold nanoparticles (AuNPs). As neither GFPβ1-10 nor GFPβ11 are independently fluorescent, the fluorescence arising from the event of their complementation would indicate the GFPβ11 decorated AuNP constructs successfully entered the cytosolic compartment of the cell after their endocytosis and endosomal escape. Note that while this design seemed feasible, we encountered numerous challenges that prevented measurement of DNA-AuNP conjugates escape. The following sections of this chapter describe some the inherent limitations of this approach.

2.2. Methods

Synthesis of GFPβ11

The GFPβ11 peptide (N'-RDHMVLHEYVNAAGIT-C') was synthesized on Rink Amide resin (Liberty, Discover, CEM Microwave Peptide Synthesizer). The peptide was cleaved from the resin by trifluoracetic acid. The cleaved peptide was precipitated in cold diethylether. The precipitants were dried overnight. The dried products were dissolved in water, flash frozen, and lyophilized. The peptide was then dissolved in 90% water: 10% acetonitrile and purified by an analytical-scale reverse-phase high-performance liquid chromatography (HPLC) with a Grace Alltech C18 column (1 mL/min flow rate; Solvent A: nanopure water + 0.05% trifluoroacetic acid, Solvent B: acetonitrile + 0.05% trifluoroacetic acid; starting condition: 90% A & 10% B). The purified peptide was confirmed through MALDI-TOF mass spectrometry using the α-CHCA matrix method

described above (4700 Proteomics Analyzer, Applied Biosystems). The purified peptide was stored in -20°C for short term and -80°C long term.

Initial in Solution Complementation of GFPβ11 with GFPβ1-10

Fluorescence arising from complementation was initially tested with HPLC purified GFPβ11 and GFPβ1-10 (Sigma Aldrich) in a 96-well plate during the course of one-hour (Cytation 5, BioTek). The controls included: 50 µM GFPβ11 and 96.5 µM GFPβ1-10 in water. These fluorescence values were used to normalize the fluorescence resulting from complementation of 50 µM GFPβ11 and 96.5 µM GFPβ1-10. The excitation/emission values are 485/520 nm.

In Solution Complementation of GFPβ1-10 with Varying Concentrations of GFPβ11

The complementation of GFPβ11, at varying concentrations, was performed with a constant concentration of 50 µM GFPβ1-10. The increase in fluorescence intensity of GFPβ11 with GFPβ1-10 was performed after allowing 24-hours to complement at room temperature and after allowing three-hours to complement at 37 ℃. The GFPβ11 concentrations tested include 0, 2, 20, 50, and 100 µM. Measurements were taken in 1x PBS (Cytation 5, BioTek).

In solution Complementation of GFPβ11-PEG:mPEG AuNPs with GFPβ1-10

50 µM thiol-PEG 2000-alkyne was conjugated through click chemistry to 95 µM GFPβ11 to create GFPβ11-PEG 2000-thiol. The click conditions were performed over three-hours with 0.5 mM THTPA, 0.1 mM $CuSO_4$, and 5 mM ascorbic acid. This product and a backfilling thiol-mPEG were added to 10 nM gold particles in a 1:29 ratio and left to conjugate for overnight with constant agitation. The fluorescence intensity of complementation arising from 5 nM particles with 50 µM GFPβ1-10, in nanopure water, was measured over one-hour at two-minute intervals (Cytation 5, BioTek).

In solution Complementation of Biotin GFPβ11 AuNPs with GFPβ1-10

Biotin GFPβ11 was made by reacting concentrated purified peptide with ~1 mg of NHS Biotin, dissolved in 10 µL of DMSO. The reaction conditions were 10 % sodium bicarbonate, 10% 10x PBS, and 60% water. The reaction was left for four-hours. The product was then purified by an analytical-scale reverse-phase HPLC with a Grace Alltech C18 column (1 mL/min flow rate; Solvent A: nanopure water + 0.05% trifluoroacetic acid, Solvent B: acetonitrile + 0.05% trifluoroacetic acid; starting condition: 90% A & 10% B). The product was confirmed through MALDI-TOF mass spectrometry using the α-CHCA matrix method described above (4700 Proteomics Analyzer, Applied Biosystems). The particles were prepared by adding concentrated Biotin GFPβ11 to gold particles (freeze method). The fluorescence of 0.825 nM particles, 1 µM Biotin GFPβ11, and 10 µM Biotin GFPβ11 were measured with 50 µM GFPβ1-10 (Cytation 5, BioTek).

2.3. Results

2.3.1. Confirmation of GFPβ11 Synthesis
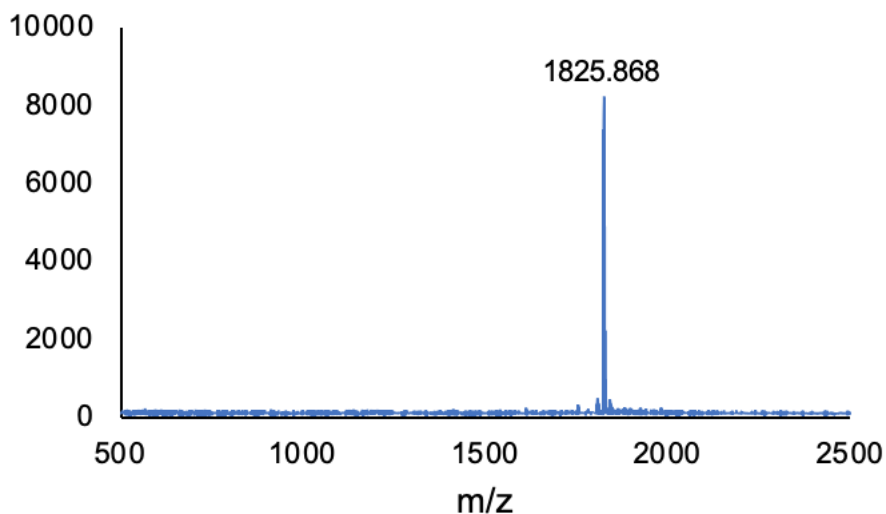
Figure 2.3. MALDI-TOF mass spectrum of GFPβ11 following its cleavage from synthesis resin and HPLC purification.

Figure 2.3. shows the MALDI-TOF mass spectrum of purified GFPβ11 following is synthesis and cleavage. The mass of GFPβ11 is 1824.8 Da. Thus, the overall mass of the product should be about 1825.8 Da which is seen in this spectrum. This peak is indicative of the 1+ species because its mass-to-charge ratio (m/z) is the same as that of the expected value.

2.3.2. Preliminary Validations of Split GFP Complementation Assay
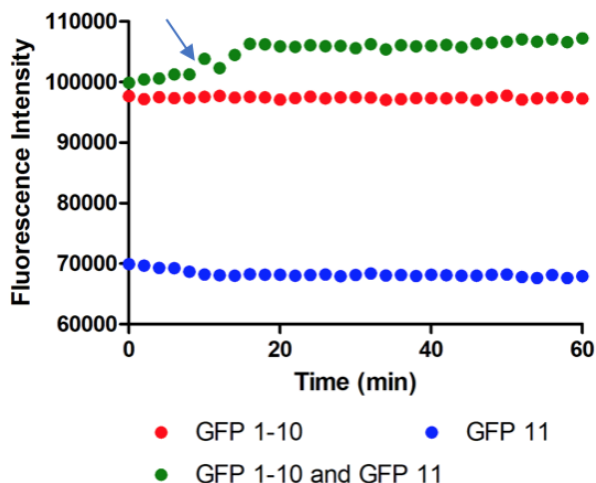
Figure 2.4. In solution complementation of GFPβ11 with GFPβ1-10. The blue line shows the fluorescence of GFPβ11 in water. The red line shows the fluorescence of GFPβ1-10 in water. The green line shows the fluorescence arising from the complementation of 50 μM GFPβ11 and 96.5 μM GFPβ1-10. The arrow points to the fluorescence increase occurring within the first 20-minutes of the reaction. This reaction was measured every two-minutes for one-hour (Cytation 5, BioTek).

Figure 2.4. shows the preliminary complementation of 50 μM GFPβ11 with 96.5 μM GFPβ1-10. The complementation was performed in water over the course of one-hour to determine kinetics of complementation (Cytation 5, BioTek). Negative controls of GFPβ11 and of GFPβ1-10 auto-fluorescence were additionally measured. The controls maintained constant fluorescence intensities. Despite the anticipation that the GFPβ1-10 only sample should not be fluorescent, it did exhibit fluorescence intensity levels about 1.4-times more intense than that of the GFPβ11 only sample.

The sample containing both, GFPβ1-10 and GFPβ11, did show an increase in fluorescence intensity within the first 20-minutes of the complementation reaction, as indicated by the arrow. After 20-minutes, the fluorescence intensity plateaued at a 1.6-fold more intense fluorescence intensity than that of GFPβ11. Fluorescence intensity was measured every two-minutes (Cytation 5, BioTek). The next experiment presented was instead performed in 1x PBS and included a variety of GFPβ11 concentrations, in an effort to address the limited fluorescence intensity observed.
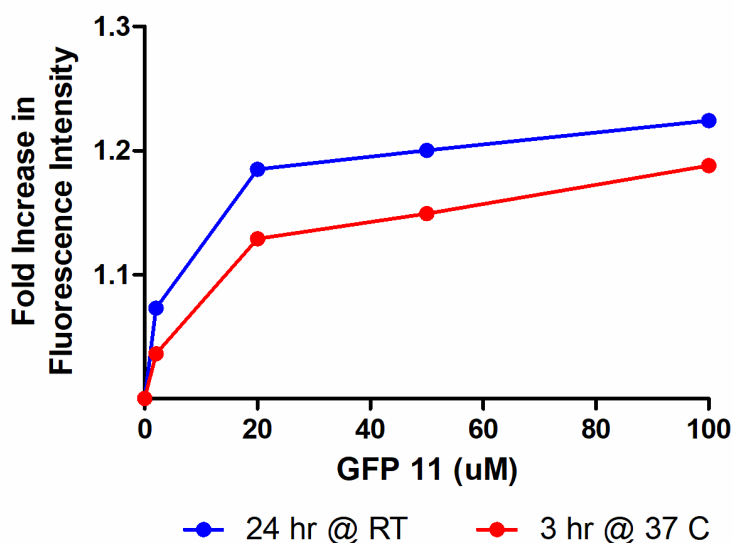
Figure 2.5. The complementation of GFPβ11, at varying concentrations, and 50 μM GFPβ1-10. The blue line shows the fold increase in fluorescence intensity of GFPβ11 with GFPβ1-10 after allowing 24-hours to complement at room temperature, as a function of GFPβ11 concentration (0, 2, 20, 50, 100 μM). The red line shows the fold increase in fluorescence intensity of GFPβ11 with GFPβ1-10 after allowing three-hours to complement at 37 ℃, also as a function of GFPβ11 concentration. Measurements were taken in 1x PBS (Cytation 5, BioTek).

Figure 2.5. illustrates the fluorescence intensity of unmodified GFPβ11 after extended complementation reaction time with GFPβ1-10 (Cytation 5, BioTek). The reactions were left for either 24-hours at room temperature or for three-hours at 37 ℃. The concentration of GFPβ1-10 was 50 μM in 1x PBS and the concentration of GFPβ11 was varied (0, 2, 20, 50, 100 μM).

As seen in **Figure 2.5.**, the fluorescence intensity increases with increasing GFPβ11 concentration. All 24-hour duration complementation reaction intensities were greater than that of the three-hour long reactions. The fluorescence intensity, for 24-hours, was only about 1.2-fold greater for the 100 μM GFPβ11 when compared to 0 μM GFPβ11. Considering the maximum fold increase (of 1.2), the sensitivity of this assay is very poor. Nonetheless, we continued to investigate this assay by conjugating GFPβ11 to PEG 2000 in order to functionalize gold nanoparticles and test its complementation capabilities.

2.3.3. Validation of Split GFP Complementation on AuNPs
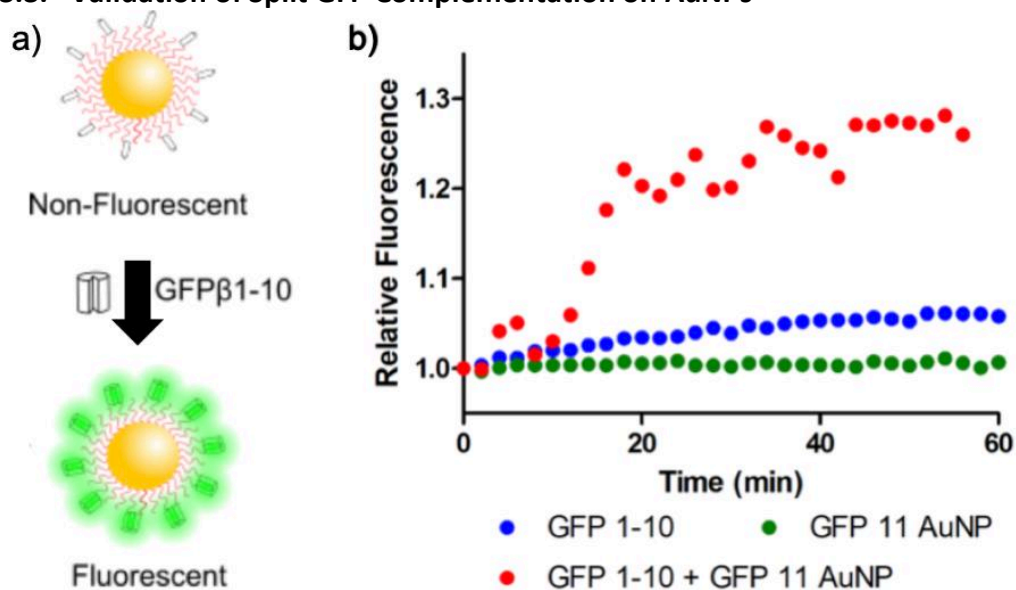
Figure 2.6. In solution complementation of GFPβ11-PEG:mPEG AuNPs with GFPβ1-10. (a) shows the general reaction scheme: 5 nM GFPβ11-PEG:mPEG AuNPs were made in a 1:29 ratio and added to 50 μM GFPβ1-10 to measure fluorescence intensity. (b) The normalized fluorescence intensity of the particles is shown by the green line. The normalized fluorescence of 50 μM GFPβ1-10 is represented by the blue line. The red line shows the complementation reaction of the particles with GFPβ1-10. The three samples were measured in nanopure water for one-hour in two-minute intervals (Cytation 5, BioTek).

Despite the limited fluorescence intensities observed in **Figures 2.4. & 2.5.**, we continued to test the fluorescence intensity of a GFP complementation. Gold nanoparticles functionalized with GFPβ11-PEG and mPEG were created to test complementation on particles. **Figure 2.6.** illustrates

the complementation-mediated fluorescence of these GFPβ11-tagged gold nanoparticles in nanopure water. This experiment was performed with negative controls of GFPβ1-10 and of GFPβ11-PEG:mPEG functionalized AuNPs. **Figure 2.6.a.** shows a schematic of these particle's synthesis. The functionalized particles were made by incubating 10 nM AuNPs with a 1:29 mixture GFPβ11-PEG:mPEG, overnight, at final concentration of 1 µM and 29 µM, respectively.

As illustrated by **Figure 2.6.b.**, the complementation does result in a fluorescence intensity increase over the one-hour timeframe. The majority of complementation events occur in the first 20-minutes, after which point the fluorescence intensity continues to increase but a slower rate. After about 40-minutes, the fluorescence intensity completely levels off. A 1.14-fold enhancement of fluorescence is seen when compared to the GFPβ1-10 group. The fluorescence intensities of the groups were normalized to the fluorescence of each sample at the initial timepoint (t=0). Fluorescence measurements were taken every two-minutes for one-hour (Cytation 5, BioTek).

2.4. Discussion

As seen in **Figures 2.4.-2.6.**, complementation events do indeed result in an increased fluorescence intensity. However, the fluorescence arising from complementation is not as great as reported previously.[48] Specifically, Lönn e al. reported a 30-fold enhancement in fluorescence upon complementation of GFPβ1-10 with GFPβ11. The difference in observed enhancement is likely due to a number of reasons.

Firstly, fluorescence enhancement is limited by the number of complementation events that can occur on the nanoparticle surface. We roughly estimate that each particle is limited to 16 complementation events. This value is based on the minimal size differences between our 13 nm

particles and the 4.2 x 2.4 nm dimensions of a complete GFP β-barrel, as well as, based on the 1:29 ratio of GFPβ11-PEG-to-backfilling mPEG. Other ratios of GFPβ11-PEG:mPEG were also tested, but complementation-based fluorescence increases were similar or less than those shown in **Figure 2.6.b.** (data not shown). Moreover, alternative methods for linking GFPβ11, including the use of a biotin/streptavidin connection to the linker and the use of a DNA linker were explored. We were unable to increase the effectiveness of the GFP complementation reaction through these methods.

Secondly, the signal of these complementation events is further limited by gold's absorption spectral overlap with that of GFP's emission. 13 nm gold nanoparticles have a spectral absorbance peak at 520 nm. The ~510 nm emission of GFP, therefore, does result in signal quenching. This quenching was admittedly anticipated, however, the unforeseen and proposed steric limitations, in tandem with quenching, results in exceedingly low levels of fluorescence.

Figure 2.4. shows GFPβ1-10 to have an auto-fluorescent signal which was not reported by references.[48] Therefore, there may also be issues with the starting peptide and the GFPβ1-10 protein obtained from commercial sources. This additional signal would add to background and noise to further skew confidence in fluorescence signals reported. Furthermore, because cells are auto-fluorescent themselves, we concluded that although this assay's simplistic design has proven to be effective in other studies, it will not be sensitive enough to use for future studies of endosomal escape by DNA-AuNP conjugates in cells.

2.5. Conclusions

Based on the poor sensitivity of the GFP complementation assay, we decided to abandon this approach. In the following chapter, the development of a ratiometric pH-sensitive assay is

discussed and its application to test known endosomal escape enhancing proteins is currently being investigated.

Chapter 3: Quantifying Endosomal Escape Using a Ratiometric pH-Sensitive Assay

3. **Quantifying Endosomal Escape Using a Ratiometric pH-Sensitive Assay**

    3.1. Background and Design

    After an unsuccessful attempt to develop an assay to quantitatively define nanoparticle location within cells through a split GFP complementation strategy, the design of the assay was altered to no longer rely on fluorescent proteins, but rather was redirected to make use of fluorescent dyes as inspired by a Hammond et al. paper. In their work, they developed an assay to detect the intracellular location of dual-layer silica nanoparticles. The inner layer, or core, was created by covalently bonding ATTO647N to a silane precursor of silica and the outer layer by similarly bonding fluorescein isothiocyante (FITC).[36] ATTO647N is pH insensitive: its fluorescence is not affected by pH and remains constant in various environments.[36] FITC, on the other hand, is a pH-sensitive dye: its fluorescence intensity is dependent on the pH of the environment in which it resides.[36] By ratiometrically comparing the two fluorescence signals, they were able to determine relative location of their particles within cells.[36]

    Earlier, we noted a recently published pH-sensitive ratiometric NP probe named the pH-BOT (pH-sensing bio-optical transponder). The probe was developed on 6.6 nm gold particles and relies on three fluorescent dyes: fluorescein amidite (FAM), DyLight 405 (DL405), and DyLight 700 (DL700).[35] Although all three dyes are pH-sensitive, the DyLight dyes are nearly pH insensitive at physiological pH ranges, but still are susceptible to slight change. Two ratios are tabulated (FAM:DL405 and DL405:DL700). The probe also uses the plasmonic ruler technique of surface energy transfer between two of the dyes (FAM and DL405) and the particle surface. The three dyes are conjugated to a DNA duplex which is anchored to the particles. The gold particle core quenches FAM and DL405 while the DNA-AuNP construct is intact but has no such quenching

effect on DL700. The change in the DL405:DL700 fluorescence intensity ratio is dependent on the

DNA duplex's conjugation to the Au core. The change in the FAM:DL405 fluorescence intensity

ratio is dependent on environmental pH. Thus, the probe reports on DNA-AuNP uptake, changing

environmental pH during intracellular trafficking, and DNA cargo release.[35]

Although the pH-BOT probe appears to accomplish much of what we wish to do with our own

particles, our design differs in several aspects and is tailored to be applied to our catalytically

active 13 nm Dz-AuNPs. Because their probe is reliant on 6.6 nm particles and a DNA duplex,

neither characteristic is particularly valuable for our own single-stranded, 13 nm DNA-AuNP

conjugate investigations. Furthermore, a limitation, or unnecessary complication, of their design

is their use of three pH-sensitive dyes. It is true that FAM is the most pH sensitive of the three

and that the other two are only mildly sensitive, but all respond to pH changes which inherently

complicates their model. Below we describe a dual-labeled DNA-AuNP probe that relies on only

one pH-sensitive dye.
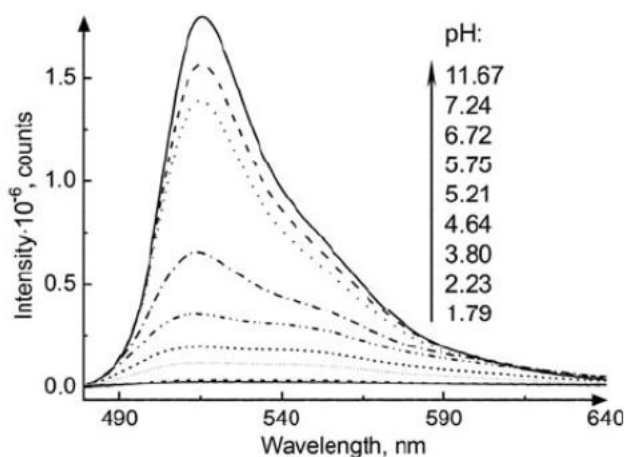
Figure 3.1. The fluorescence emission of fluorescein (5' 6-FAM) at varying pH. Adapted from *Russian Phys. J.*[51]

Herein, the assay described utilizes two different fluorescent chromophores: fluorescein amidite, 5' 6-FAM (or FAM), and ATTO647N. These dyes were selected based on several opposing characteristics. ATTO647N is a red fluorescent dye with excitation/emission values of 647/661 nm. It is cationic and can be conjugated to ssDNA through NHS-amine chemistry. FAM, like FITC is a green fluorescent dye and has excitation/emission values of 495/520 nm.[52] It is an anionic dye that can be conjugated to ssDNA. As seen in **Figure 3.1.**, FAM is a highly pH-sensitive dye whose fluorescence intensity increases with increasing pH.[52] The sensitivity is attributed to its three protonatable oxygens with pK_a values of 2.2, 4.3, and 6.7.[35]
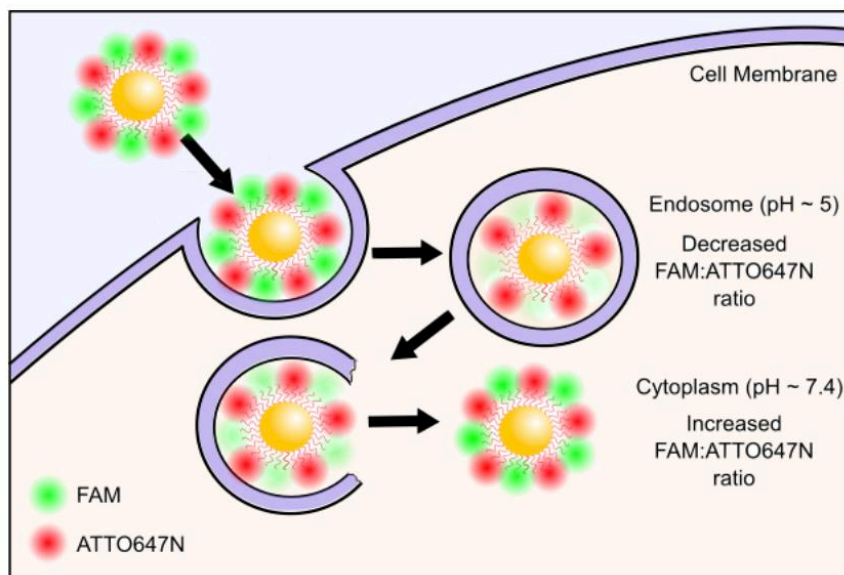
Figure 3.2. Schematic to show 5'6-FAM fluorescence signal decrease as a result of lower pH within endosome upon DNA-AuNP uptake by cells through endocytosis. As figure describes, cytosolic pH ~7.4 while endosomal pH ~5. Figure also shows FAM fluorescence signal increase upon DNA-AuNP escape from endosome.

Figure 3.2. illustrates the design of the ratiometric pH-sensing assay we have been working to develop. If the two dyes are functionalized to the same AuNP in known concentrations, their fluorescence ratio in solution, which varies as a function of pH, can be used to develop a standard curve. This standard curve should then be capable to extrapolate the environmental pH the

particles occupy. An in-cell standard curve was developed by manipulating cellular pH with a HEPES/MES buffer spiked with sodium azide which results in proton pump obstruction and thereby enables cell pH modulation. Because endosomal pH ($\sim$5-6) is notably different from cytosolic pH ($\sim$7.4), the ratio of FAM to ATTO647N fluorescence should discern the location of the particles when introduced to cells.

3.2. Methods

ATTO647N conjugation to DNA-T20 and Purification

NHS-ATTO647N (Sigma Aldrich) was conjugated to T20-sequence, single-stranded DNA with a 5' amine and 3' thiol (IDT). 50 mg of NHS-ATTO647N was dissolved in 10 µL of DMSO and reacted with 10 nmol of amine-T20-thiol in 1x PBS with 0.1 M NaHCO$_3$. The reaction was left over night. The following day, excess dye was removed by P2 gel filtration (Nanosep MF Centrifugal Devices) and purified using an analytical-scale reverse-phase HPLC with an Agilent Advanced oligo column (0.5 mL/min flow rate; Solvent A: 0.1 M TEAA, Solvent B: acetonitrile; starting condition: 90% A & 10% B).

Transmission Electron Microscopy (TEM)

The size distribution of 5 nM T20 AuNPs and 5 nM FAM/ATTO647N/T20 AuNPs, suspended in nanopure water and cell culture media, was analyzed using a Hitachi H7500 transmission electron microscope. The particles were prepared by freeze method. Particles were allowed to dry on TEM grid for one-hour before imaging.

Characterization of Particle Size through Dynamic Light Scattering (DLS)

The size distribution of 5 nM T20 AuNPs and FAM/ATTO657N/T20 AuNPs, suspended in 1x PBS, was analyzed using dynamic light scattering (Nano Plus zeta/nano particle analyzer, Particulate

Systems). Normalized intensity distribution was measured and compiled from 5 replicates of 10 measurements each.

FAM/ATTO647N AuNP Fluorescence Intensity in Varying pH Buffers

The fluorescence of 4:1 FAM/ATTO647N AuNPs in varying pH phosphate-citrate buffer was measured at pHs of 4, 4.4, 5, 5.4, 6, 6.4, 7, and 7.4 (using capabilities of Monolith NT.115Pico miscroscale thermophoresis instrument). The particles were prepared by freeze method and upon final resuspension, after centrifugation, the particles were introduced to the different buffers. The buffers were prepared by mixing different volumes of 0.2 M Na_2HPO_4 and 0.1 M citrate based on published protocols.

DTT DNA Release Assay

1 mL of 4:1 FAM/ATTO AuNPs were prepared through the freeze method. Following final spin of wash, particles were resuspended in 200 μL of TE buffer. 5 nM of FAM/ATTO647N AuNPs were reacted with 1, 10, and 100 μM DTT (mixed 100 μL of 10 nM particles with 100 μL of 2, 20, 200 μM of DTT dissolved in TE buffer). Fluorescence of reaction was monitored by measuring FAM and ATTO647N signals as DNA released from particle after two-hours.[53, 54] Assay was repeated with solutions of FAM- and ATTO647N-labeled-T20 not conjugated to AuNPs. In this assay, 250 nM of FAM-labeled-T20 and 250 nM of ATTO647N-labeled-T20 (500 nM total DNA concentration) was treated with 1, 10, 100 μM DTT in TE buffer. FAM and ATTO647N fluorescence were monitored over two-hours on plate reader.

FAM/ATTO647N AuNPs in pH-Clamped Cells by HEPES/MES Buffer with NaN₃

HEK293FT cells were plated in a 24 well plate with about 40,000 cells per well and allowed to adhere overnight. Media used was DMEM prepared with 10% FBS, 2% L-glutamine, and 1%

PenStrep. 5 nM of 4:1 FAM/ATTO647N particles, prepared as described above, were introduced to wells and allowed to incubate. At 16-hours, the cells were trypsinized and centrifuged 2x at 300 rcm for 5 min, resuspending once in 1x PBS and once in 500 µL of varying pH HEPES/MES buffers and chilled on ice prior to flow cytometry (LSR II, Becton Dickinson). The buffers were prepared at pHs of 4, 5, 5.8, 6.2, 6.8, and 7.4 by mixing 5 mM HEPES and 50 mM MES containing 50 mM NaCl, 30 mM ammonium acetate, and 40 mM sodium azide (this protocol was adapted from Hammond et. al). pHs were checked using a pH meter.

FAM/ATTO647N/T20 AuNPs in Cells

HeLa cells were plated in a 24-well plate with about 40,000 cells per well and allowed to adhere overnight. 4:1:2.5 concentration FAM/ATTO647N/T20 particles, prepared as described above, were introduced to wells and allowed to incubate for four-hours. Following the four-hour pulse with nanoparticles, the media (DMEM 10% FBS, 2% L-glutamine, and 1% PenStrep.) was replaced with non-nanoparticle containing media and left unchanged for the remainder of the treatment. Following pulse-chase treatment, the cells were trypsinized and washed three-times. Washes consisted of centrifugation for five-minutes at 300 rcm, three-times, resuspending in 1x PBS after each centrifugation, with final resuspension in 500 µL of 1x PBS. The cells were then chilled on ice prior to flow cytometry (LSR II, Becton Dickinson). The effects of chloroquine were tested as well by incubating HeLa cells with FAM/ATTO647N/T20 AuNPs alongside 100 µM chloroquine.

Fluorescence Microscopy

Cleaned 25 mm glass slides by sonicating for 20 min in 50% ethanol. Slides were then rinsed with nanopure water repeatedly to ensure no ethanol remained. Slides were then treated with piranha solution (25% hydrogen peroxide, 75% sulfuric acid) for five-minutes and then rinsed

with nanopure water many times and allowed to dry in oven. Chambers for glass slides were similarly cleaned by sonicating for 20-minutes in 50% ethanol and then dried in oven. Finally, imaging chambers were assembled by carefully placing glass slides into cleaned, dried chambers. 4:1:2.5 FAM/ATTO647N/T20 particles were prepared through freeze method. ~50,000 HeLa were plated in each imaging chamber in 500 µL of cell media. The following day, frozen particles were thawed and washed three-times in nanopure water. The cell media in the glass chamber was replaced with fresh cell media containing 5 nM of washed particles and 10% 10x PBS was added to cells. An epifluorescence microscope was used to measure fluorescence in FAM and/or ATTO647N channels at various timepoints.

3.3. Results

3.3.1. Confirmation and Characterization of FAM-/ATTO647N-DNA AuNPs
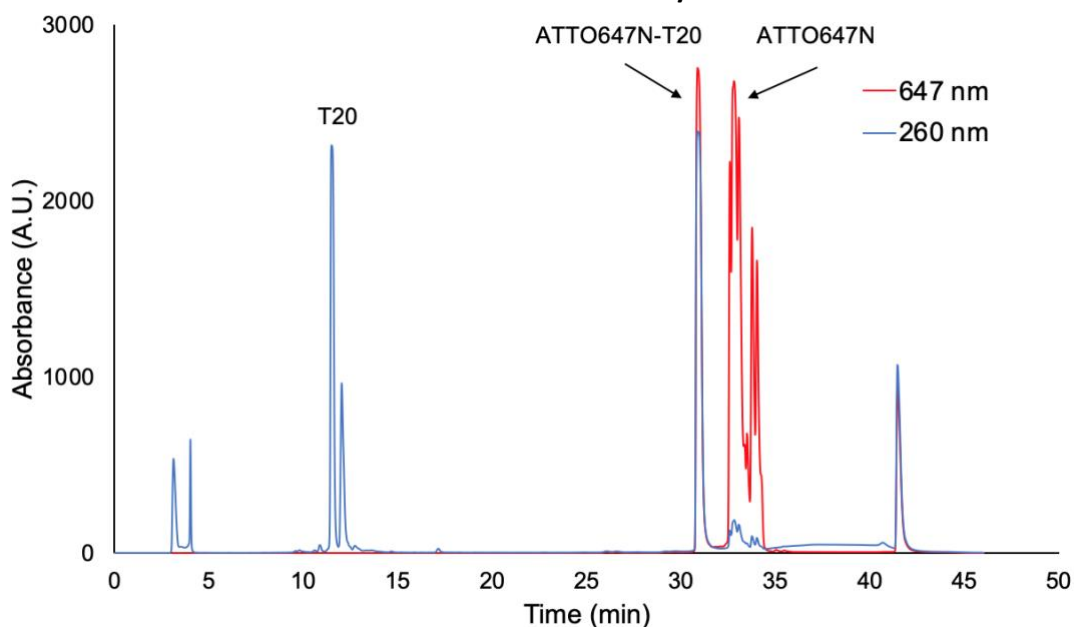

Figure 3.3. HPLC spectrum of ATTO647N-T20 DNA conjugation. The blue line shows the absorbance of DNA at 260 nm. The red line shows the absorbance of ATTO647N at 647 nm.

Figure 3.3. shows the HPLC purification of the conjugation reaction of ATTO647N with thiol-T20-amine DNA. The peak at the 31-minute elution time is indicative of the desired ATTO647N-

T20 product as both 260 and 647 nm absorbance are seen in high abundance, this peak is indicated by the first arrow. The second arrow, points to a peak containing both 260 and 647 nm absorbance, as well, but the low intensity of the 260 nm signal indicates that this is unlikely to be the desired ATTO647N-T20 conjugate. Following this synthesis, we made what will be referred to as ATTO647N/FAM/T20 AuNPs. These particles consist of a gold core NP, with three types of DNA functionalized to them: the ATTO647N labeled T20 DNA (just discussed in **Figure 3.3.**), FAM labeled T20 DNA (purchased from IDT), and unlabeled T20 DNA. We then went on to characterize and confirm the stability of these triply-conjugate DNA AuNPs.
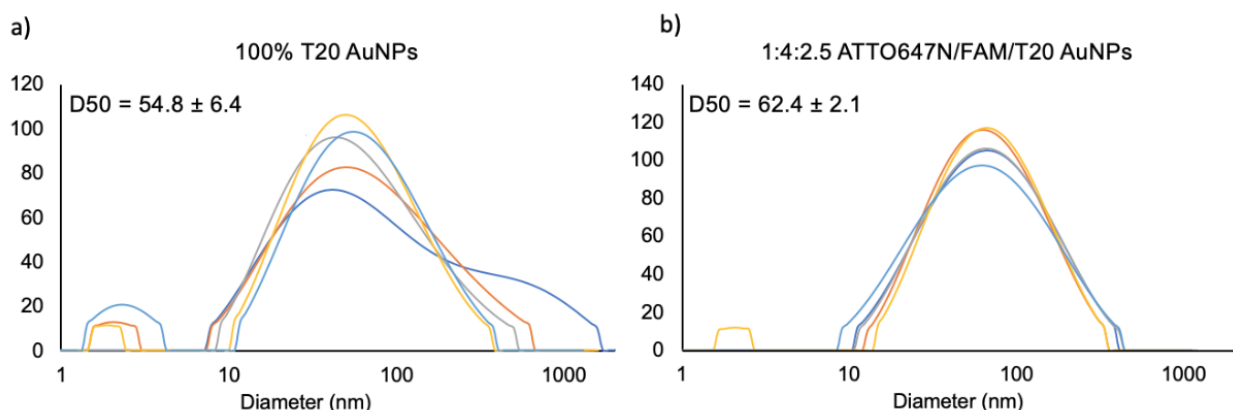
Figure 3.4. (a) Intensity weighted size distribution curve of 13 nm T20-only gold nanoparticle conjugates as measured through dynamic light scattering. **(b)** Intensity weighted size distribution curve of 13 nm 1:4:2.5 ratio ATTO647N/FAM/T20 AuNP conjugates as measured through DLS. Legends contain the median diameter (D50) values with standard deviation from the five trials. The x-axis is a logarithmic scale and the DLS was performed in 1x PBS.

Figure 3.4. shows the DLS obtained intensity weighted size distribution of two batches of particles. Both samples were measured five-times, indicated by the five curves on each plot. Both batches of particles were prepared at 5 nM in 1x PBS. The legends include the median diameter (D50) values measured. The x-axis is a logarithmic scale. **Fig. 3.4.a.** shows the distributions for gold nanoparticles conjugated with only T20 DNA. **Fig. 3.4.b** shows the distributions for gold nanoparticles with ATTO647N-T20 DNA, FAM-T20 DNA, and T20 DNA conjugated in a 1:4:2.5

ratio. The D50 value for the triply-conjugated AuNPs was larger than that of the T20-only particles, which is to be expected because of the addition of the dyes should increase the overall particle diameter. The relatively minimal broadening of the histograms indicates that there is little to no aggregation of the particles. To further confirm their stability, we used transmission electron microscopy.
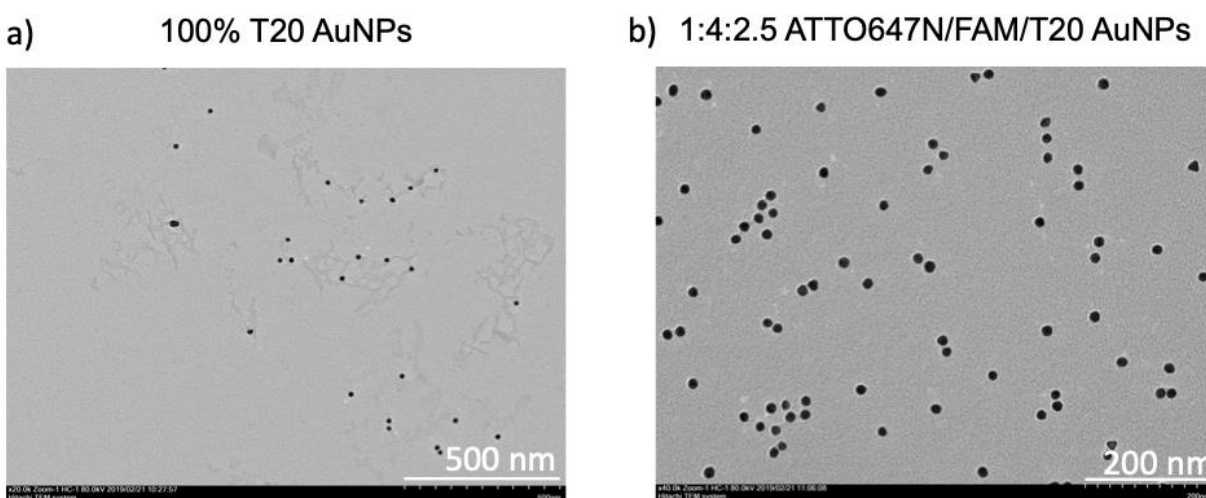
Figure 3.5. (a) Transmission electron microscopy image of 13 nm, 5 nM T20-only AuNPs suspended in nanopure water with a 500 nm scale bar. **(b)** Transmission electron microscopy image of 13 nm, 5 nM ATTO647N/FAM/T20 AuNPs (in a 1:4:2.5 concentration ratio, suspended in nanopure water) with a 200 nm scale bar.

Figure 3.5. shows TEM images of **(a)** 5 nM T20-only AuNPs and of **(b)** 5 nM 1:4:2.5 ATTO647N/FAM/T20 AuNPs to confirm their stability. The two batches of particles were suspended in nanopure water and allowed to dry on a TEM grid for one-hour. Particles show no aggregation which indicates that they are fairly stable despite the conjugation of two ionic dyes. We then incubated triply-conjugated AuNPs in media to see its effects on stability.
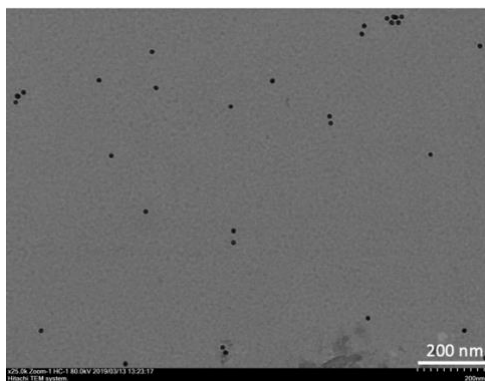
Figure 3.6. Transmission electron microscopy image of 13 nm, 5 nM ATTO647N/FAM/T20 AuNPs (in a 1:4:2.5 concentration ratio, suspended in media over 72-hours) with a 200 nm scale bar.

Figure 3.6. shows TEM image of 5 nM ATTO647N/FAM/T20 AuNPs suspended in media over 72-hours and allowed to dry for one-hour. The particles were again prepared in a 1:4:2.5 ratio. The particles show no aggregation and this image confirms that the particles can be suspended in media without compromising their stability. This provides assurance that these particles can at least be administered to cells without fear that they are aggregated. After confirmation of their synthesis and their characterization, we then introduced the particles to solutions of varying character to measure these effects on the two fluorescence intensities.

3.3.2. In Solution Manipulations and the Effect on Fluorescence
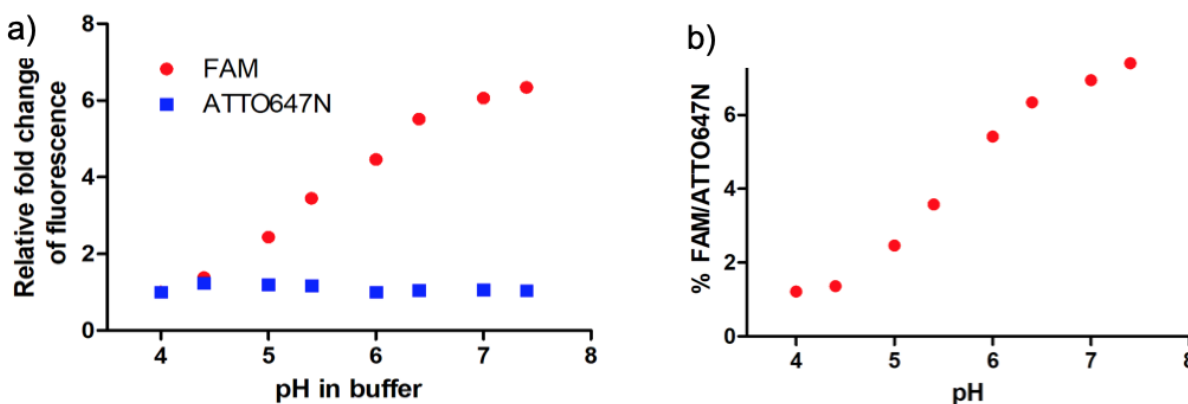
Figure 3.7. In solution FAM/ATTO647N AuNP fluorescence intensity in varying pH phosphate-citrate buffers. Citric acid/phosphate buffers of 4, 4.4, 5, 5.4, 6, 6.4, 7, and 7.4 pH units were made and the fluorescence intensity of 4:1 FAM/ATTO647N particles was measured. **(a)** shows the individual florescence intensities of FAM (red points) and ATTO647N (blue points), on

particles, as a function of pH. **(b)** shows the % FAM to ATTO647N fluorescence intensities, on particles, as a function of pH.

Figure 3.7. shows preliminary FAM and ATTO647N fluorescence intensities when conjugated to AuNPs through 3' thiolated ssDNA-dye conjugates. Here the fluorescence intensities of the FAM/ATTO647N particles was measured in phosphate-citrate solutions of varying pH. As seen in **Figure 3.7.a.**, the fluorescence intensity of ATTO647N remains fairly constant across the pH range, confirming that the dye's fluorescence intensity is in fact pH insensitive. Meanwhile, the increase in FAM fluorescence intensity with increasing pH confirms that FAM's fluorescence intensity is pH-sensitive. The fluorescence intensities of FAM and ATTO647N were normalized to the value at pH 4.

Figure 3.7.b. shows the percent FAM-to-ATTO647N fluorescence ratio. This ratio was computed by dividing the fluorescence intensity of FAM by that of ATTO647N and multiplying by 100%. This was done because the raw signal of ATTO647N is much more intense than that of FAM. As illustrated by the sigmoidal-like plot, the ratio increases with increasing pH. The ratio value at pH 5, or what is characteristic of endosomes, is roughly 2.5%, while the ratio value at pH ~7.4, which is characteristic of cellular cytoplasm, is roughly 7%. Therefore, there is roughly a 3-fold enhancement in percent FAM-to-ATTO647N signal from pH ~7.4 in comparison to pH 5. The distinguishable difference at endosomal-characteristic pH and cytoplasm-characteristic pH, in solution, provides reassurance for their in-cell application. We then tested the effects of DTT on fluorescence intensities, as a method of mimicking the DNA-cargo release by AuNP which reportedly occurs within endosomes.[30, 35, 53, 54]
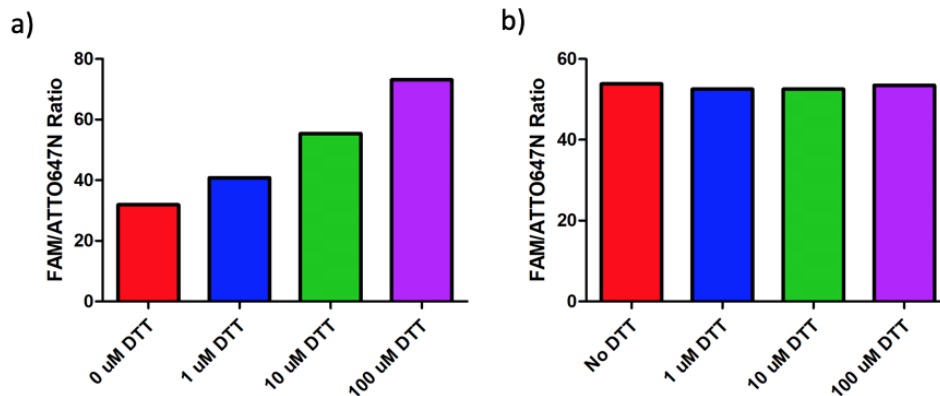
Figure 3.8. (a) FAM/ATTO647N fluorescence ratio arising from 4:1 5nM FAM/ATTO647N AuNPs suspended in TE buffer after reacting with varying concentrations of DTT (0, 1, 10, 100 μM) for two-hours. **(b)** FAM/ATTO647N fluorescence ratio arising from 1:1 500nM total soluble FAM- and ATTO-DNA conjugates not functionalized to NPs, suspended in TE buffer after reacting with varying concentrations of DTT (0, 1, 10, 100 μM) for two-hours.

Due to the expected difference arising from AuNP-based quenching of FAM, the FAM/ATTO647N ratio was compared for DNA-dyes conjugated to particles and DNA-dyes in solution. Therefore, **Figure 3.8.** shows the effects of DTT, at varying concentration, on the FAM/ATTO647N fluorescence intensity ratio for 4:1 5nM FAM/ATTO647N AuNPs **(Fig. 3.8.a.)** and for soluble FAM- and ATTO647N-DNA conjugates which were prepared in a 1:1 ratio with a total DNA concentration of 500 nM **(Fig. 3.8.b.)**. DTT is used to displace thiolated oligonucleotides from gold nanoparticles.[53, 54] Both plots show the fluorescence ratios of the different conditions (0, 1, 10, 100 μM DTT) after a two-hour exposure. In **Fig. 3.8.a.**, the FAM/ATTO647N fluorescence intensity ratio increases with increasing DTT concentration, from 30 to 75 fluorescence ratio. The increase in the fluorescence ratio that arises from increasing DTT concentration, confirms DNA displacement off AuNPs.

Figure 3.8.b. shows the FAM/ATTO647N fluorescence intensity ratio for the soluble DNA-dye conjugates remains independent of DTT concentration. The conjugates were also exposed to DTT for two-hours, exposed to the same concentrations of DTT as the dye-labelled DNA-AuNPs, and

was also performed in TE buffer. The soluble DNA-dye solution was prepared in a 1:1 ratio of FAM:ATTO647N with a total concentration of 500 nM DNA-dye.

The increase in the FAM/ATTO ratio that arises from increasing DTT concentration, suggests that the FAM/ATTO647N ratio is sensitive to DNA displacement from the gold nanoparticle surface. This fact suggests that the experimental ratios measured will only be accurate as long as the dye-DNA-particle construct is intact and will be considered in the design of future experiments. We then set off to test our pH-sensing particles in manipulated cells.

3.3.3. In Cell Manipulations and the Effect on Fluorescence
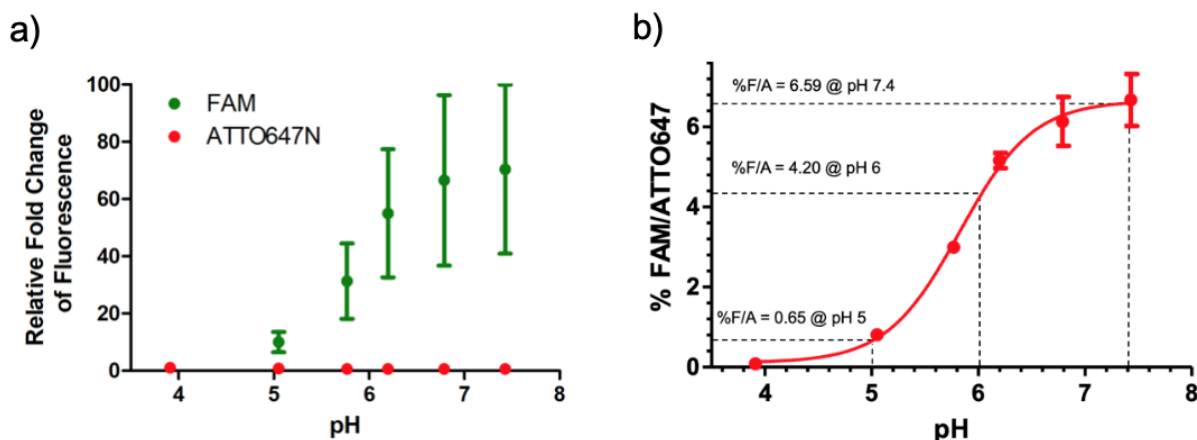
Figure 3.9. FAM/ATTO647N AuNPs in HEK293FT cells with HEPES/MES with NaN$_3$ buffer. **(a)** The individual fluorescence of ATTO647N is represented by red points. The individual fluorescence of FAM is represented by green points. **(b)** The relative fluorescence of 4:1 FAM/ATTO647N AuNPs was measured using flow cytometry to produce this standard curve. HEPES/MES buffers were made with pH values of 4, 5, 5.8, 6.2, 6.8, and 7.4. FAM/ATTO647N fluorescence ratio as a function of pH.

Figure 3.9.a. shows the baseline subtracted and normalized fluorescence signals from the FAM (green points) and ATTO647N (red points) dyes on 4:1 FAM/ATTO647N AuNPs in pH-clamped HEK293FT cells. The baseline fluorescence, or control, signal was measured in cells that were not treated with nanoparticles. The cells were incubated in a pH-clamping HEPES/MES buffer spiked with sodium azide. Sodium azide causes proton pump obstruction and enables

cellular pH modulation. The pHs tested include of 4, 5, 5.8, 6.2, 6.8, and 7.4. As seen in the in-solution results (**Figure 3.7.**), the FAM fluorescence signal increases with increasing cellular pH while ATTO646N remains largely unchanged.

Figure 3.9.b. shows the relative percent FAM-to-ATTO647N fluorescence ratio of these AuNPs. The figure confirms that even in cells, the FAM/ATTO647N fluorescence ratio increases with increasing pH and continues to do in a sigmoidal-like manner. At pH 7.4, the ratio (of 6.59%) is roughly 10-times larger than that of pH 5 (0.65%). The curve was fit with a Boltzmann sigmoidal curve equation: $\left(\%\text{FAM/ATTO647N} = 0.1087 + \frac{6.5513}{1+e^{\frac{(5.826-\text{pH})}{0.3424}}} \right)$. Note: here we used HEK293FT cells and have since moved to HeLa cells, therefore, this standard curve requires replication in our new cell model.
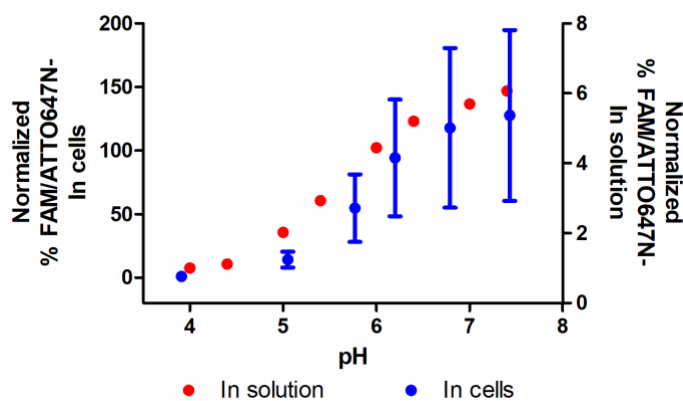
Figure 3.10. Overlay of **Figures 3.7.b. & 3.9.b.** Red points show normalized FAM/ATTO647N ratio of particles in pH varying solutions (pHs of 4, 4.4, 5, 5.4, 6, 6.4, 7, and 7.4). Blue shows normalized FAM/ATTO647N ratio of particles in pH clamped cells (pHs of 4, 5, 5.8, 6.2, 6.8, and 7.4).

Figure 3.10. shows an overlay of the in solution and in cell standard curves developed from **Figures 3.7.b. & 3.9.b.** This was done in order to more easily compare the in-solution percent FAM-to-ATTO647N fluorescence ratios to that of the pH-clamped HEK293FT cells. The overlay

shows that the two curves are consistent for in solution and in cells experiments, where the

FAM/ATTO647N ratios increase with increasing pH and begin to level off around pH of 7.

3.3.4. pH-Sensing AuNPs in Cells
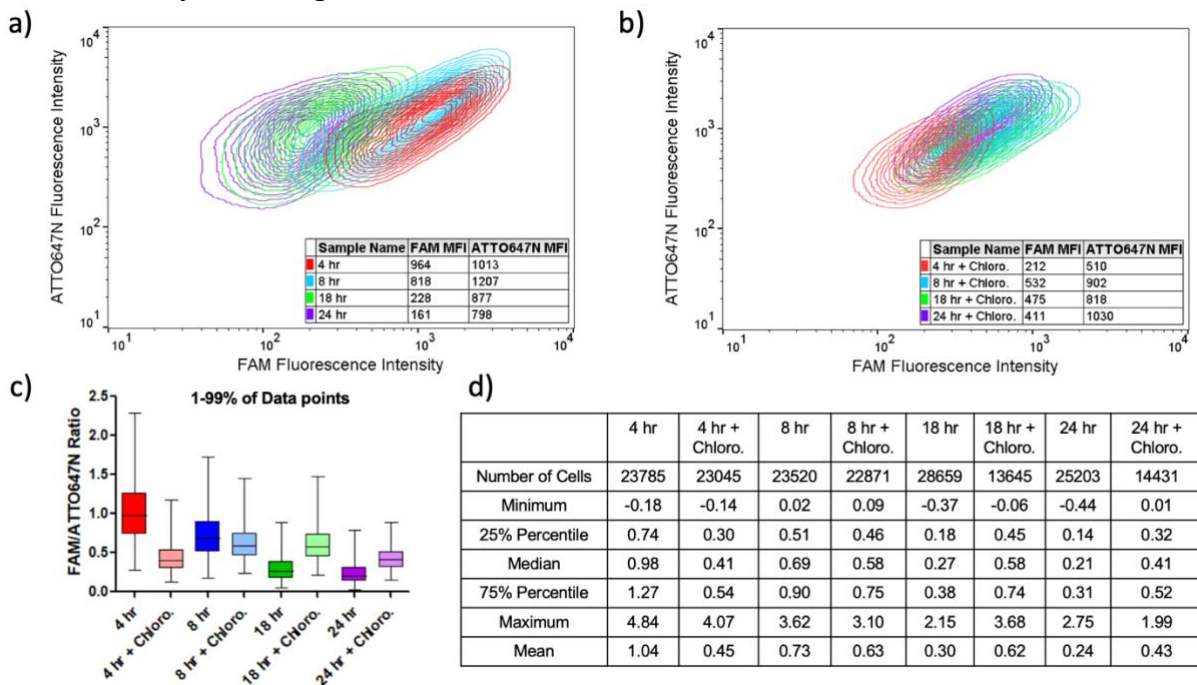
Figure 3.11. 5 nM 1:4:2.5 ATTO467N/FAM/T20 AuNPs incubated in HeLa cells for four-hours and chased for the remainder of time post incubation. Additionally, cells with the same timepoints were treated with 100 µM chloroquine. **(a)** a density dependent map of FAM versus ATTO647N fluorescence intensities for the varying timepoints of cells not treated with chloroquine. **(b)** a density dependent map of FAM versus ATTO647N fluorescence intensities for the varying timepoints of cells that were treated with chloroquine. **(c)** a histogram of the relative percent FAM/ATTO647N ratio for all cell groups with the top and bottom one percent of data points removed. **(d)** shows the number of cells and the fluorescence signals of the: minimum, 25th percentile, median, 75th percentile, maximum and mean for all cell groups.

Figure 3.11. shows the fluorescence intensity of FAM and ATTO647N, as measured by flow

cytometry in HeLa cells (the previous cell experiments had been performed in HEK293FT cells, so

the standard curve developed cannot be directly applied to this data and an updated standard

curve experiment is in progress). The cells were pulsed/treated for four-hours with 5 nM 1:4:2.5

ATTO647N/FAM/T20 AuNPs and chased for the remainder of the experiment. Additionally, cells

with the same timepoints and particle exposure were treated with 100 µM chloroquine. **Figures**

3.11.a. & 3.11.b. both show a density dependent map of the FAM versus ATTO647N fluorescence signals for cells treated at varying timepoints. **Fig. 3.11.a.** shows cells that were not exposed to chloroquine while **Fig. 3.11.b.** shows the effects of chloroquine incubation. In both sections, the ATTO647N signal remains fairly constant (around 10^3 arbitrary fluorescence units). In **Fig. 3.11.a.** there is an apparent decrease in FAM signal as a function of increasing time. In the chloroquine exposed cell groups (**Fig. 3.11.b.**) there is a less cohesive trend: the FAM signal is lowest for the 4-hour group, followed by the 18-, 8-, and 24-hour groups.

Fig. **3.11.c.** shows a histogram of the relative FAM/ATTO647N ratios for all cell groups with the top and bottom one percent of data points removed. As portrayed by the raw data of **Fig. 3.11.a.**, the overall fluorescence ratio for cells decreased with increasing time in non-chloroquine exposed cells. Meanwhile, as portrayed by the raw data of **Fig. 3.11.b.**, the fluorescence ratio of chloroquine treated cells followed no such time-dependence. When comparing the fluorescence ratios of the 4- and 8-hour timepoints, the chloroquine-treated groups exhibited decreased fluorescence ratios. Meanwhile, when comparing the 18- and 24-hour timepoints, the fluorescence ratios increase in the chloroquine treated cell groups. In brief, the FAM fluorescence of AuNP-only treated cells follows a time-related trend while the chloroquine-AuNP treated groups did not.

Fig. **3.11.d.** shows the number of cells measured in each experimental group. It also includes the fluorescence signals of the minimum, 25th percentile, median, 75th percentile, maximum, and mean for all cell groups. For groups at later timepoints and chloroquine exposure, the number of cells measured was significantly lower, despite more growth time. The 18-hour cell population was more than twice as large in the non-chloroquine treated group than in the chloroquine

treated group. Chloroquine is a weak base that is able to buffer acidic cellular vesicles and used to aid in transfection of nonviral vectors, but it is also known to be cytotoxic (which is why we do not wish to use it as an endosomal escape enhancer).[36, 55]
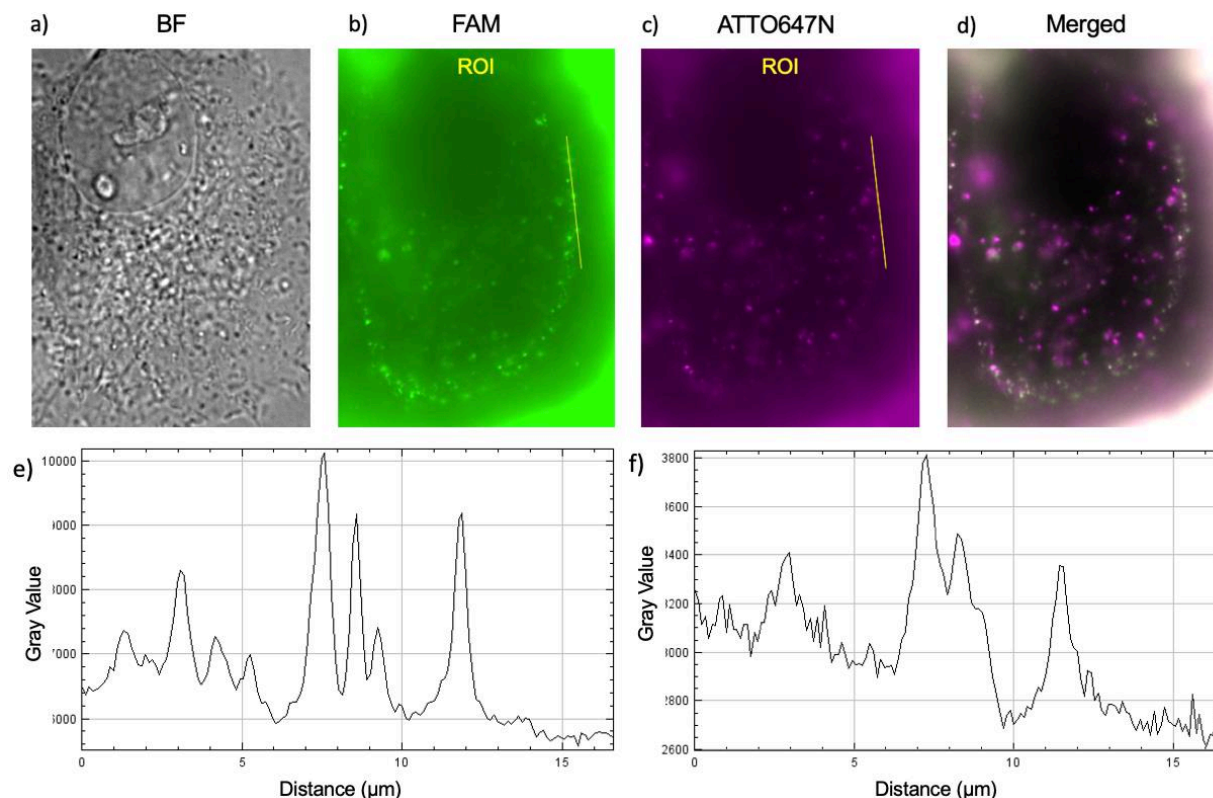
Figure 3.12. Fluorescence microscopy images of 5 nM 1:4:2.5 ATTO467N/FAM/T20 AuNPs incubated in HeLa cells for four-hours. **(a)** shows the brightfield. **(b)** shows the FAM channel. **(c)** shows the ATTO647N channel. **(d)** shows an overlay of the two channels. **(e)** the line scan from FAM. **(f)** the line scan from ATTO.

Figure 3.12. contains six components: four of which include the microscopy images of one cell from different imaging channels **(a-d)** and the other two components show line scans **(e, f)**. Cells were transfected with 5 nM ATTO647N/FAM/T20 AuNPs (prepared in a 1:4:2.5 ratio) for 4-hours. **Fig. 3.12.a.** shows the brightfield image of a cell. **Figures 3.12.b. & 3.12.c.** show the FAM and ATTO647N channels, respectively, for the same cell. Both contain a line scan to measure individual fluorescence signals. **Fig. 3.12.d.** shows an overlay of the FAM and ATTO647N

channels. **Figures 3.12.e. & 3.12.f.** contain the gray value intensity of the line scans from **Figures 3.12.b. & 3.12.c.**

Sections (b-d) show many fluorescence puncta in both the FAM and ATTO647N channels. The overlay shows good colocalization of these puncta **Fig. 3.12.d.** In the overlayed signal, it appears that puncta closer to the edge of the cell have stronger FAM intensity (appearing greener), whereas puncta further from the edge of the cells have diminished FAM intensity (appearing more purple). This observation is consistent with an endocytosis-mediated uptake mechanism, where early endosomes, primarily located on the edge of the cell, have higher pH. At this higher pH, the FAM signal should be greater. The pH of late endosomes is typically lower, they are characteristically located further within the cell, and because of lower pH, FAM signal should be decreased. Admittedly, there is a significant background in both channels, which is likely a result of not up-taken particles non-specifically interacting with the glass cover slip.

As seen in **Figures 3.12.e. & 3.12.f.**, there is good overlap in the distance values (represented by the major peaks) from the line scans. The peaks indicate location along the line scan of individual fluorescence puncta and the strong overlap suggests that the FAM and ATTO647N puncta arise from the same location. Based on these images alone, they suggest that the particles either remain intact within the endosome or the DNA cargo has been released but remains within the endosome.

3.4. Discussion

This chapter discussed the ongoing development of a ratiometric pH-sensing DNA-AuNP probe. The probe was made possible by determining a ratio of two fluorescent dyes, fluorescein (FAM) and ATTO647N, conjugated to thiolated single-stranded DNA. These thiolated ssDNA-dye

complexes were then functionalized to 13 nm gold nanoparticles. The design of the probe was based on one inherently differing characteristic of the two dyes and was inspired by Hammond et al.[36] The noteworthy difference between the two dyes is that the fluorescence intensity of FAM is directly related to pH dependent, while the fluorescence intensity of ATTO647N is pH independent. The pH dependence of FAM is attributed to its three protonatable oxygen groups.[35] For this reason, a ratio of FAM-to-ATTO647N fluorescence intensity can be helpful in determining pH.

Using commercially available FAM-T20 DNA-thiolate, synthetically conjugated ATTO647N-T20 DNA-thiolate, and unlabeled 3' thiolated DNA T20, we developed and characterized a tri-DNA conjugated AuNP pH-sensing probe. The ATTO647N-DNA-thiolate synthesis was confirmed through HPLC techniques as shown in **Fig. 3.3.** The stability and characterization of our pH-sensing NP probes was confirmed through dynamic light scattering in 1x PBS (**Fig. 3.4.**) and through transmission electron microscopy (**Figures 3.5. & 3.6.**). DLS showed an overall increase in the median diameter (D50) for ATTO647N/FAM/T20 AuNPs, by 7.6 nm, from that of the T20 DNA-only AuNP controls. The relative diameter values, for the two groups, indicates that there is no apparent particle aggregation. Furthermore, any apprehension of aggregation is diminished by the minimal broadening of the DLS plots. Images from TEM also corroborate particle stability in both nanopure water and cell culture media.

With the reassurance of stable particles, we then tested the pH-dependence of FAM and pH-independence of ATTO647N by introducing our particles to phosphate-citric acid buffers at variant pHs. The fluorescence intensities of FAM and ATTO647N were then measured and confirmed that as pH increases, so too does FAM's fluorescence intensity and that the

fluorescence intensity of ATTO647N remains largely unaffected. There was an apparent 3-fold enhancement in the FAM-to-ATTO647N signal regarding pHs 7.4 and 5. The effect of changing in-solution pH can be seen in **Fig. 3.7.** where the pHs tested ranged from 4-7.4 pH units as a means to mimic the various pH environments our DNA-AuNPs could encounter if incubated in cells.

Following the investigation of pH effect on fluorescence intensity in-solution, we tested the effects of DTT. DTT acts as a method to displace thiolated-DNA from gold and is used to mimic the DNA-cargo release that occurs within endosomes by DNA-AuNPs.[30, 35, 53, 54] The DTT release assay (**Fig. 3.8.**) showed that the FAM-to-ATTO647N fluorescence ratio of our AuNPs does increase with increasing DTT concentration while the soluble FAM-to-ATTO647N fluorescence ratio remains unchanged with increasing DTT concentration. The respective rise and independence of fluorescence ratios suggests that the gold core construct of our probes does introduce inherent uncertainty in our design because of quenching that arises in the spherical probe. If in the event the thiol-gold bond, formed by the thiolated ssDNA, is degraded and the ssDNA dissociates from the core, the intensity of FAM fluorescence increases. Future work will need to be done to address this limitation in our design.

We continued to investigate our probes within cells and began to do so by introducing them to HEK293FT cells with modulated pH. The cells were incubated with our probes and the fluorescence intensities of FAM and ATTO647N were measured in a pH-clamping solution of HEPES/MES buffer spiked with sodium azide (**Fig. 3.9.**). Again, the pH range was based on expected intracellular ranges (pH 4-7.4). The assay followed the sigmoidal trend seen in the in-solution experiment and found that the fluorescence ratio at pH 7.4 is roughly 10-times greater than the ratio at pH 5. To further clarify and impart the resemblance of **Figures 3.7. and 3.9.**, we

provided an overlay (**Fig. 3.10.**). From this it is very easy to see the shared sigmoidal trend of FAM's fluorescence dependence on pH. Because the subsequent in cell experiments were performed in a different cell model, we will need to reperform this experiment to create a standard curve that is applicable to the new cell type.

With our standard curve partially developed, we began introducing our pH-sensing NP probes to HeLa cells without experimental manipulation. The fluorescence intensity of ATTO647N and FAM was measured in cells by flow cytometry, that were pulsed for four-hours with the NP probes, after chasing for 0-, 4-, 14-, and 20-hours (**Fig. 3.11.**). Additionally, the effect of chloroquine on fluorescence was tested. We found, as expected, the intensity of ATTO647N to be independent of time for all cell exposure types. We also anticipated and found that the intensity of FAM decreased as a function of incubation time for cells treated with particles but not treated with chloroquine.

When the pH-clamping standard curve (**Fig. 3.9.b.**) was applied to the in-cell flow cytometry experiment (**Fig. 3.11.**) (and the difference in cell lines used for the two experiments is ignored), we found that the median pH reported by the particles was 4.40 pH units at the 24 hr time point. This value was calculated from the ratio value of 0.21 and the Boltzmann sigmoidal curve equation (provided in **Results 3.3.2.**). This highly acidic pH value implies that the vast majority of DNA-AuNPs are within late endosomes after 24-hours of incubation. This value also implies that very little DNA cargo release is occurring. If significant release were occurring, the FAM/ATTO647N ratio would be enhanced and resulting in a higher pH value because FAM fluorescence would no longer be quenched by the AuNP. Given that the measured pH approaches the most acidic reported values in the literature, this strongly suggests that there is little DNA-

release from the AuNP scaffold that would bias the measurement away from more acidic environments. Endosomes and even lysosomes maintain pHs above 4 pH units.

Additionally, when we apply the standard curve (**Fig. 3.9.b.**) to the chloroquine treatments (**Fig. 3.11.b-d.**), we note that chloroquine appears to aid in endosomal escape for the 18 and 24 hr time points. The median FAM/ATTO647N ratio values suggest that at early points (4 hr), chloroquine leads to DNA-AuNP environments that are more acidic than that of the non-treated group. At later time points (8 hrs), the median FAM/ATTO647N ratio suggests little difference in pH between the chloroquine treated group and the non-treated group of cells. At the 18 and 24 hr time points, the median FAM/ATTO647N ratio suggests that the chloroquine leads to endosomal escape (increase in the pH) of the DNA-AuNP. This result is consistent with the literature as chloroquine is known to enhance endosomal escape. In future work, we will repeat the pH-clamp experiment in HeLa cells to confirm the conclusions reported here.

Finally, we performed fluorescence imaging microscopy within HeLa cells to confirm our flow cytometry findings (**Fig. 3.12.**). The cell images presented were of cells that had been incubated with our pH-sensing DNA-AuNPs for four-hours. Visual assessment of the FAM and ATTO647N fluorescence puncta found good colocalization of the two signals, which indicates uptake mediated through endocytosis. Visual assessment also found the majority of puncta events to be at the edge of the cell. This is consistent with the four-hour incubation period as cells are expected to reside in early endosomes that are characteristically found near the membrane of the cell. Line scans from the FAM and ATTO647N further confirm colocalization of puncta and reaffirm that endosomal escape has not yet taken place at this timepoint.

The findings presented here regarding the steps toward developing a pH-sensitive 13 nm single-stranded DNA-gold nanoparticle are quite promising. And although, replicates are required and many more experiments necessary, we are quite confident in our pH-sensing AuNP probe at this point in its development. Indeed, reproduction of the pH-clamped standard curve in our new cell line, as well as replication of the flow cytometry and microscopy with additional timepoints are necessary. Additionally, we believe the chloroquine treatment of cells should be investigated at greater depth. Further study of the effects of DTT would, also, be very beneficial in understanding and addressing the DNA-cargo release that inevitably occurs by DNA-AuNPs within endosomes.

3.5. Conclusions

This chapter contained various forms of findings to validate the development of a pH-sensing 13 nm single-stranded DNA-gold nanoparticle. We would like to reaffirm and improve these preliminary results by re-performing, in-triplicate, several experiments. After successfully completing the development of this assay, we hope our probes can be useful in testing known endosomal escape enhancing peptides. The following chapter describes the potential design of an endosomolytic-DNA AuNP that utilizes our finalized pH-sensing probe to test their efficacy.

Chapter 4: Steps Toward Screening Endosomal Escape Enhancing Peptides

Author Contributions

K.M.J. and B.R.D. designed this project, performed these experiments, and analyzed this data. All contributors discussed results and gave input on manuscript.

4. Endosomal Escape Enhancing Peptides

4.1. Background and Design

Endosomal entrapment, and by extension insufficient delivery, of DNA-gold nanoparticle conjugates is a major constraint of the activity of DNA-AuNPs.[34] Accordingly, this limits the activity of Dz-AuNPs, as described in our recent works, and their potential efficacy in biomedical applications,.[10, 23, 24] In order to address entrapment of DNA-gold nanoparticle conjugates, we first needed to develop a high-throughput assay to aid in determining location and trafficking of these particles within cells. The assay we have been working to develop relies on the fluorescence intensity ratio of pH-sensitive fluorescein amidite (FAM) and pH insensitive ATTO647N. After successfully developing ratiometric pH-sensing DNA-AuNP conjugates, we hope to apply these probes to screen known endosomal escape enhancing amino acid sequences. Herein, we discuss the selection, synthesis, characterization, and future investigations for four such sequences.

EEDs, or endosomal escape domains, are short amino acid sequences known to overcome the rate-limiting step of endosomal escape.[48] They are inspired by peptide transduction domains (PTDs), or cell penetrating peptides (CPPs), which are designed to deliver biomacromolecules to cells through their insertion into the cellular membrane and, thereby, stimulating endocytosis. PTDs/CPPs can have various characteristics but often are highly cationic and contain hydrophobic amino acid residues.[56] In an attempt to mimic entry into cells by viruses, the design of EEDs, PTDs, and CPPs are akin to that of virulent pathogens that contain hydrophobic residues which are believed to be responsible for their successful cellular transfection.[48, 56] Unlike CPPs and PTDs, EEDs are designed only to rupture the lipid bilayer of endosomes and keep the cell's plasma membrane intact. The two sequences we have selected to screen contain several hydrophobic

residues (GFWFG and GWWG). These sequences were selected because they reported the greatest endosomal escape when tested in a split GFP assay.[48]

In addition to screening EEDs, we have also decided to screen two antimicrobial peptides (AMPs). AMPs are membrane-active sequences, derived from multicellular organisms, that penetrate microbial membranes as a means to provide defense.[57, 58] Some AMPs exhibit amphipathic structures that are believed to be responsible for membrane disruption. An environment-responsive reorganization of the hydrophobic, hydrophilic, and cationic amino acids results in these dual-component structures.[58-60] AMPs are known to be endosomolytic and minimally toxic.[57] These characteristics may be essential for accomplishing our goal: to develop endosomolytic DNA-AuNPs that have little to no adverse effects on the cell's overall integrity. The two AMP sequences we have selected to screen include Aurein 1.1 (GLFDIIKKIAESI-Cys.) and Aurein 1.2 (GLFDIIKKIAESF-Cys.). They showed the greatest escape of several AMPs.[57]
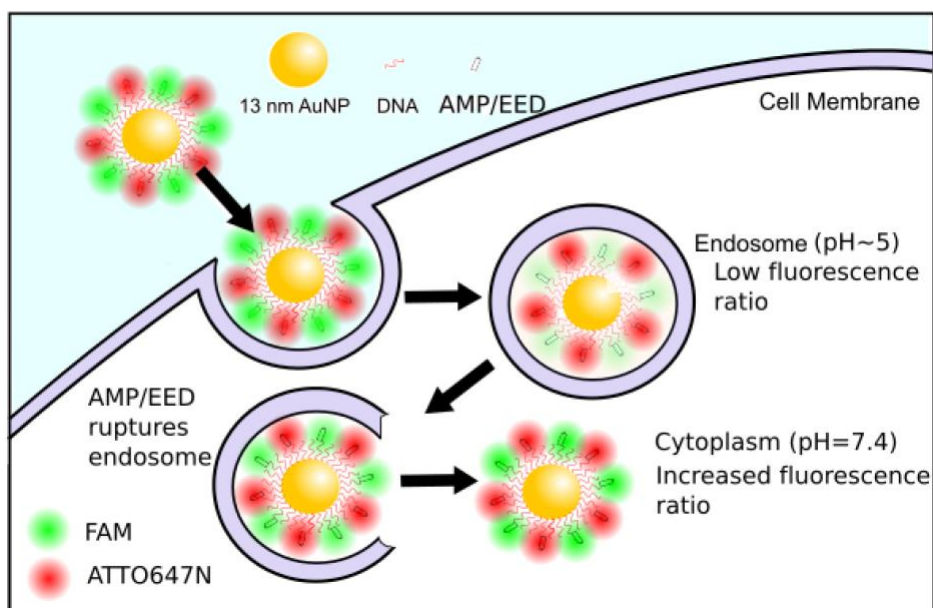

Figure 4.1. Schematic to show FAM fluorescence signal decrease as a result of lower pH within endosome upon DNA-AuNP uptake by cells through endocytosis. As figure describes, cytosolic pH ~7.4 while endosomal pH ~5. Figure also shows FAM fluorescence signal increase, and

therefore ratio increase, upon DNA-AuNP escape from endosome through AMP/EED induced endsomolysis.

As seen in **Figure 4.1.**, we plan to screen the four sequences by covalently linking the peptides to thiolated ssDNA through either: sulfo-SMCC chemistry for the AMPs or NHS-azide followed by click chemistry for the EEDs. This T20 DNA-peptide conjugate, in addition to our two dye-DNA conjugates, will be functionalized to gold nanoparticles so that the three DNA conjugates create FAM/ATTO647N/peptide DNA-AuNPs. The concentration of FAM/ATTO647N/peptide will exist in the same ratios as our FAM/ATTO647N/T20 DNA-AuNPs, developed in Chapter 3. The standard curves (**Fig. 3.9. & 3.10.**) should be useful for extrapolation the cellular location of these particles and measuring the individual escape enhancement by the four peptides.

4.2. Methods

Synthesis of AMPs and EEDs

The peptides Aurein 1.1 (N'-GLFDIIKKIAESI-Cys.-C') and Aurein 1.2 (N'-GLFDIIKKIAESF-Cys.-C') were synthesized on Fmoc-Cys(Trt)-Wang resin (0.629 mMol/g, Sigma Aldrich) (Liberty, Discover, CEM Microwave Peptide Synthesizer). Domains 1 (N'-GFWFG-C') and 2 (N'-GWWG-C') were synthesized on Rink Amide resin (Liberty, Discover, CEM Microwave Peptide Synthesizer). The two Aurein peptides were cleaved and deprotected using a cleavage cocktail of 92.5% trifluoroacetic acid, 2.5% 1,2-Ethanedithiol, 2.5% triisopropylsilane, and 2.5% water. The shorter two sequences have not been cleaved and are currently under storage in a -80°C freezer. The two cleaved peptides were then precipitated in cold diethylether. These precipitants were dried overnight. The dried products were dissolved in water, flash frozen, and lyophilized. The peptides were then dissolved in 90% water: 10% acetonitrile and purified by an analytical-scale reverse-

phase HPLC with a Grace Alltech C18 column (1 mL/min flow rate; Solvent A: nanopure water + 0.05% trifluoroacetic acid, Solvent B: acetonitrile + 0.05% trifluoroacetic acid; starting condition: 90% A & 10% B). The two purified peptides were confirmed through MALDI-TOF mass spectrometry using the α-CHCA matrix method described above (4700 Proteomics Analyzer, Applied Biosystems). The purified peptides are stored in -30°C for short term and -80°C long term.

Conjugation of Aurein 1.2 to DNA-T20

HPLC purified Aurein 1.2 was conjugated to a T20-sequence, single-stranded DNA (IDT) through a sulfyl-SMCC reaction (Thermo Scientific). A reaction solution of 50% water, 20% 20 mM stock of sulfo-SMCC, 20% 1 mM T20 DNA, and 10% 10x PBS was left at room temperature for 45-minutes. The unreacted sulfo-SMCC was removed with P2000 gel. The remaining solution was then added to the HPLC purified peptide and left to react overnight. The product was purified using an analytical-scale reverse-phase HPLC with an Agilent Advanced oligo column (0.5 mL/min flow rate; Solvent A: 0.1 M TEAA, Solvent B: acetonitrile; starting condition: 90% A & 10% B). The product, intermediate product, and starting materials were confirmed through MALDI-TOF mass spectrometry using the 3-hydroxypicolinic acid matrix method described above (4700 Proteomics Analyzer, Applied Biosystems).

4.3. Results

4.3.1. Confirmation of AMP Syntheses

Figure 4.2. HPLC spectrum of Aurein 1.1 purification after synthesis and cleavage from resin. The product's elution time is represented by the three peaks at 37-40 minutes.

Figure 4.2. shows the HPLC purification of Aurein 1.1 following its synthesis and cleavage from

an Fmoc-Cys(Trt)-Wang resin. The three peaks at the 37-40-minute elution time are indicative of

the desired and purified peptide.
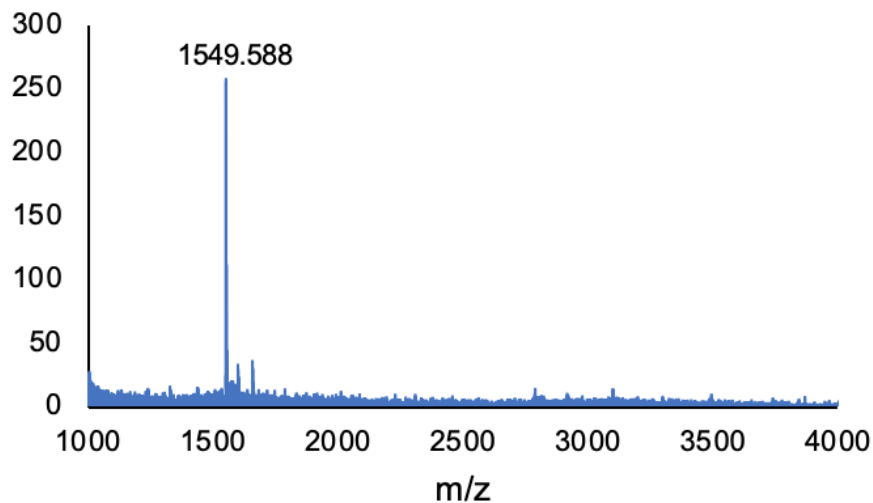
Figure 4.3. MALDI-TOF mass spectrum Aurein 1.1 following its HPLC purification (product collected from 37-40 minutes of elution).

Figure 4.3. shows the MALDI-TOF mass spectrum of purified Aurein 1.1 following is synthesis, cleavage, HPLC purification. The mass of Aurein 1.1 is 1548.9 Da. Thus, the overall mass of the 1+ charge species should be about 1549.9 Da which is seen in this spectrum.
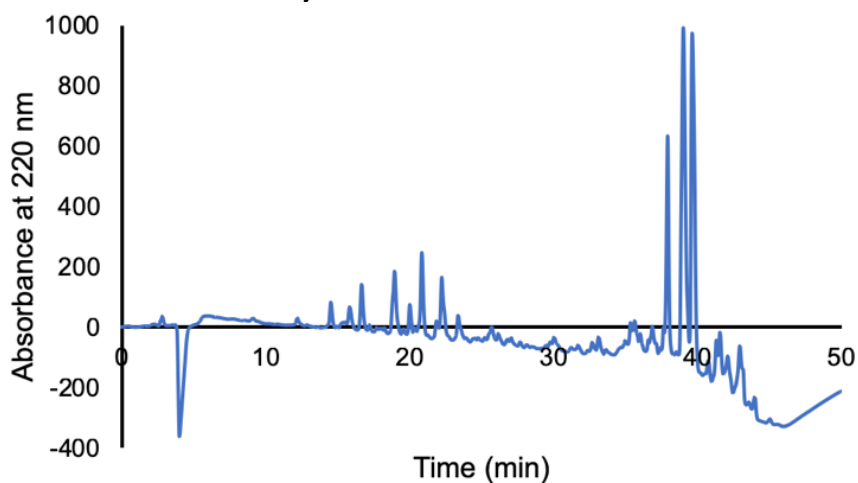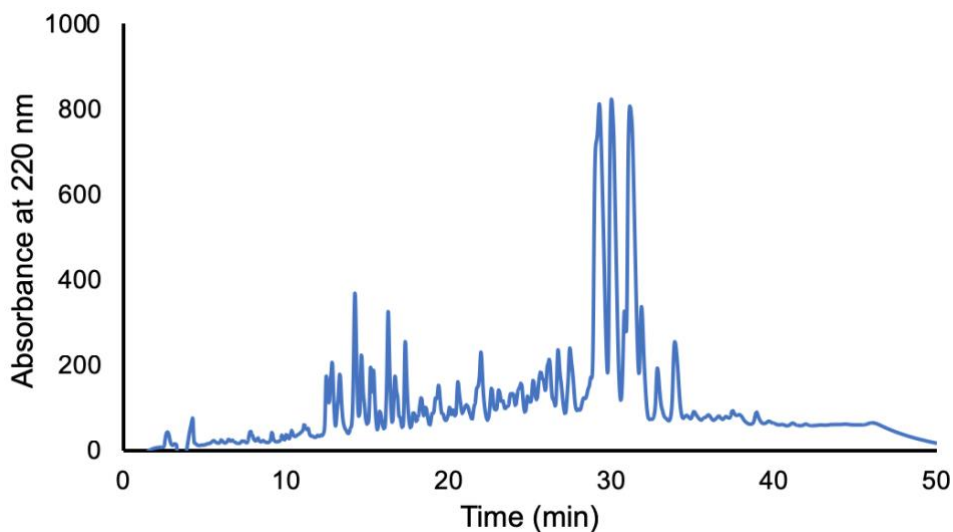

Figure 4.4. HPLC spectrum of Aurein 1.2 purification after synthesis and cleavage from resin. The product's elution time is represented by the three peaks at 29-31 minutes.

Figure 4.4. shows the HPLC purification of Aurein 1.2 following its synthesis and cleavage from an Fmoc-Cys(Trt)-Wang resin. The three peaks at the 29-31-minute elution time are indicative of the desired and purified peptide. Although **Figures 4.2. & 4.4.** are HPLC purification spectra for very similar peptide sequence (who only differ by one amino acid), the elution times differ quite drastically. This can be explained by the modification of the HPLC solvent gradient for **Figure 4.4.** The gradient was modified to increase solvent B (99.95% ACN, 0.05% TFA) earlier and more quickly so that the peptide would elute at an earlier timepoint.
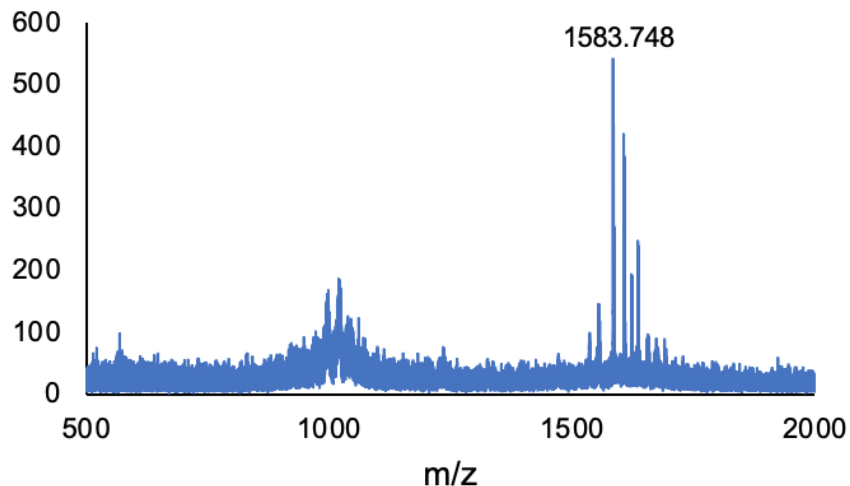
Figure 4.5. MALDI-TOF mass spectrum Aurein 1.2 following its HPLC purification (product collected from 29-31 minutes of elution).

Figure 4.5. shows the MALDI-TOF mass spectrum of purified Aurein 1.2 following is

synthesis, cleavage, HPLC purification. The mass of Aurein 1.2 is 1582.8 Da. The overall mass of

the 1+ charge species should be about 1583.8 Da. The mass-to-charge ratio seen here confirms

the synthesis of Aurein 1.2. Following the confirmation of proper synthesis, we conjugated Aurein

1.2 to T20 DNA through a sulfo-SMCC linker so that the peptide may be functionalized to our pH-

sensing particles and act as an endosomal escape enhancer.

4.3.2. Confirmation of Linking AMP to DNA
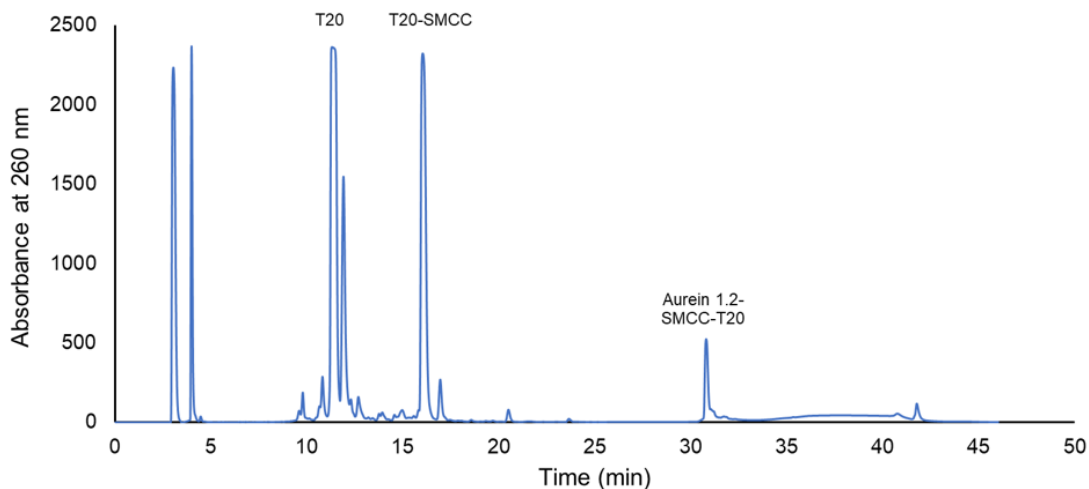
Figure 4.6. HPLC spectrum of Aurein 1.2 conjugated to T20 DNA the sulfo-SMCC chemistry. The peak at 13-minutes contains unreacted T20 DNA, the peak at 16-minutes contains the SMCC-T20

DNA intermediate, and the peak at 31-minutes contains the desired Aurein 1.2-SMCC-T20 DNA product.

Figure 4.6. shows the HPLC purification of Aurein 1.2 conjugated to T20 DNA through sulfo-SMCC chemistry. The desired product elutes at 31-minutes, as indicated in the figure. The unreacted T20 DNA and SMCC-T20 DNA intermediate elute at 13- and 16-minutes respectively. The amine of T20 DNA displaces the sulfo-NHS group of SMCC to give the intermediate. The intermediate's maleimide moiety, from SMCC, reacts with the cysteine's thiol on the peptide to give the desired product.
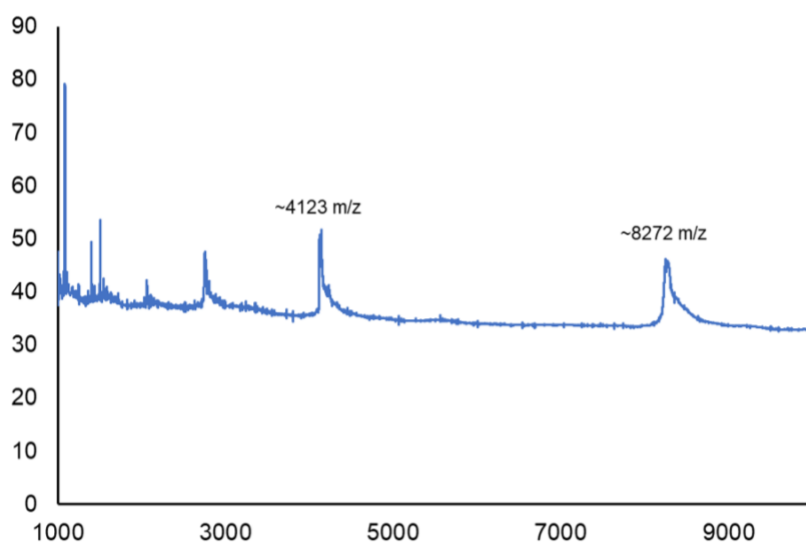
Figure 4.7. MALDI-TOF mass spectrum of Aurein 1.2-SMCC-T20 DNA product following HPLC purification.

Figure 4.7. shows the MALDI-TOF mass spectrum of purified Aurein 1.2 conjugated to T20 DNA through sulfo-SMCC chemistry. The mass of Aurein 1.2 is 1549 Da, the mass of sulfo-SMCC is 436 Da, the mass of the displaced sulfo-NHS moiety is about 194 Da, and the mass of T20 DNA is 6446 Da. Thus, the overall mass of the product should be about 8237 Da. Therefore, the peak with a mass-to-charge ratio (m/z) of 8272 confirms the synthesis of Aurein 1.2-SMCC-T20 DNA.

The charge of this peak is z=1+ and there is 0.4% error when compared to the expected mass. The peaks with a mass-to-charge ratio of 4123 is indicative of the 2+ charge species.

4.4. Discussion

Although in its early development, we are excited by the potential implications our endosomal escape enhancing DNA-AuNP constructs will have. Results from high-performance liquid chromatography (**Fig. 4.2. & 4.4.**) and MALDI-TOF mass spectrometry (**Fig. 4.3. & 4.5.**) provide confirmation of the proper synthesis of our Aurein 1.1 and Aurein 1.2 peptides. We then were able to confirm the linking of Aurein 1.2 to thiolated T20 DNA, through sulfo-SMCC chemistry (**Fig. 4.6. & 4.7.**). We ultimately hope to confirm the synthesis of the two EED sequences selected and link them to thiolated T20 DNA so that they, too, may be functionalized to particles.

After we have completed all replicates necessary to prove the robustness of our pH-sensing DNA-AuNP probes (steps detailed in Chapter 3's Discussion), we expect to continue using the 1:4:2.5 ratio design of our pH-sensing probes and will replace the unmodified T20 DNA sequence with that of our peptide-modified T20 DNA. We then will be able to screen the four different known endosomal escape enhancing sequences we have selected (Aurein 1.1, Aurein 1.2, and the two EEDs) in an effort to improve the cellular delivery of DNA-gold nanoparticle conjugates and overcome endosomal entrapment. Based on the preliminary chloroquine treatments in Chapter 3 (**Fig. 3.11.b.**), the endosomal escape enhancing DNA-AuNPs should also result in an increased FAM/ATTO647N fluorescence ratio as compared to the unmodified pH-probes. The ratio increase should be comparable to that of chloroquine's effect for an Aurein 1.2 modified DNA-AuNP.[57] Ultimately, once we have determined a sufficiently improved particle, we will adapt

this design into a DNAzyme species. In doing so, the catalytic activity of previously published Dz-AuNPs will be significantly enhanced.[10, 23, 24] These developments will not only benefit our lab's work, but it will also greatly contribute to the debate proposed by Lëvy and others.[30-34] We will shed light on the intracellular trafficking of 13 nm ssDNA-AuNPs and address the inherent limitations currently accompanied by endosomal uptake.

4.5. Conclusions

This chapter discussed the recent start to developing DNA-gold nanoparticles with enhanced endosomal escape capabilities. These enhanced nanoparticles will be screened by our pH-sensing DNA-AuNPs. The work is currently at its infancy, but four known endosomal escape enhancing sequences have been selected and synthesized. We are excited by the wide-ranging implications ssDNA-gold nanoparticles, with this feature, will have on our catalytically active particles and the field of spherical nucleic acids as a whole.

Chapter 5: Conclusions

5. Conclusions

This thesis discussed the completed and in-progress work performed by myself and my mentor, Brendan Deal, in relation to the development of a probe that is capable of determining the cellular location of 13 nm single-stranded DNA-gold nanoparticle conjugates and the adaptation of this probe to enhance DNA-AuNP delivery. The first chapter contained extensive background about the field of spherical nucleic acids with a focus on oligonucleotide-AuNPs. The introduction discussed the various applications of this nanotechnology. These applications include SmartFlares, a method of detecting intracellular mRNA levels; an RNAi-AuNP, to treat recurrent GBM; and an asDNA-AuNP, to treat psoriasis. Inherent challenges this technology faces are also discussed; namely, endosomal entrapment.

The second chapter summarizes our efforts to develop a probe reliant on an adaptation of a split GFP complementation assay. The assay proved to be insensitive and we surmised it would be incapable of the sensitivity required for intracellular detection. The fluorescence enhancement we observed upon complementation of our particles with soluble GFPβ1-10 was only 1.14-fold greater than the fluorescence arising from the soluble GFPβ1-10 alone (**Fig. 2.6.**). The effects of quenching, number of complementation events, and the auto-fluorescence we would expect to encounter intracellularly, all contribute to our decision to abandon this model.

Chapter 3 summarized the ongoing investigations to develop a smart-probe capable of determining intracellular pH. This probe relies on the ratio of two fluorescent dyes: FAM (a pH sensitive dye) and ATTO647N (a pH insensitive dye). The dyes are conjugated to 3' thiolated-ssDNA and these DNA-dye conjugates are then functionalized to 13 nm AuNPs. The probe has shown promising results with regards to its ability to produce distinctly different fluorescence

ratios in varying pH environments (**Fig. 3.7., 3.9., 3.10.**), but the in cell standard curve we have so far developed (**Fig. 3.10.**) requires replication in our new cell model. Preliminary intracellular experiments have been performed (**Fig. 3.11. & 3.12.**) and suggest that this probe is indeed capable of the desired features, but these experiments do require replication in order to validate our findings. We performed preliminary calculations by applying the pH-clamped HEK cell standard curve (or, Boltzmann sigmoidal equation) to the HeLa cell flow cytometry experiments (**Fig. 3.11.**) and were able to obtain values that validate the receptor mediated endocytosis mechanism. Validation of our probe will help to clarify the current disputes regarding endosomal trafficking and entrapment.

Finally, Chapter 4 briefly introduced our design and future goals of screening endosomal escape enhancing peptides by using our pH-sensitive probe. The successful discovery of such a peptide will enormously improve the efficacy of this nanotechnology and will have major implications in current gene therapies that rely on DNA-AuNP technology.

6. Supplemental Information

6.1. Miscellaneous Methods

DNA-AuNP Conjugation Freeze Method

3-4 µM thiolated DNA is added to 10 nM, 13-nm gold particles. The solution is then vortexed and frozen in -30°C for two-hours. The particles are thawed and centrifuged three-times at 13,000 rpm for 20-minutes to remove unbound DNA. Following each wash, the supernatant is removed, and particles are resuspended in nanopure water. Adapted from Liu et al.[61]

Matrix-Assisted Laser Desorption/Ionization-Time of Flight

Peptide MALDI-TOF

A super saturated α-cyano-4-hydroxycinnaminic acid (α-CHCA) matrix was prepared in 50% acetonitrile, 49.9% water, and 0.1% trifluoroacetic acid. Peptide was dissolved in 50% acetonitrile, 49.9% water, and 0.1% trifluoroacetic acid. 1.5 µL of each solution was plated on a 144-well MALDI plate and mixed well. The plate was allowed to dry overnight and analyzed by MALDI-TOF (4700 Proteomics Analyzer, Applied Biosystems).

DNA MALDI-TOF

A super saturated 3-hydroxypicolinic acid matrix was prepared in 50% acetonitrile, 49.9% 25 mg/ml ammonium citrate, and 0.1% trifluoroacetic acid. The DNA conjugate was dissolved in 50% acetonitrile, 49.9% 25 mg/ml ammonium citrate, and 0.1% trifluoroacetic acid. 1.5 µL of each solution was plated on a 144-well MALDI plate and mixed well. The plate was allowed to dry overnight and analyzed by MALDI-TOF (4700 Proteomics Analyzer, Applied Biosystems).

References

1. Patil, M.; Mehta, D. S.; Guvva, S., Future impact of nanotechnology on medicine and dentistry. *J Indian Soc Periodontol* **2008,** *12* (2), 34-40.

2. Emerich, D. F.; Thanos, C. G., Nanotechnology and medicine. *Expert Opin Biol Ther* **2003,** *3* (4), 655-63.

3. Hillyer, J. F.; Albrecht, R. M., Gastrointestinal persorption and tissue distribution of differently sized colloidal gold nanoparticles. *J Pharm Sci* **2001,** *90* (12), 1927-36.

4. Jensen, S. A.; Day, E. S.; Ko, C. H.; Hurley, L. A.; Luciano, J. P.; Kouri, F. M.; Merkel, T. J.; Luthi, A. J.; Patel, P. C.; Cutler, J. I.; Daniel, W. L.; Scott, A. W.; Rotz, M. W.; Meade, T. J.; Giljohann, D. A.; Mirkin, C. A.; Stegh, A. H., Spherical nucleic acid nanoparticle conjugates as an RNAi-based therapy for glioblastoma. *Sci Transl Med* **2013,** *5* (209), 209ra152.

5. Seferos, D. S.; Giljohann, D. A.; Hill, H. D.; Prigodich, A. E.; Mirkin, C. A., Nano-flares: probes for transfection and mRNA detection in living cells. *J Am Chem Soc* **2007,** *129* (50), 15477-9.

6. Mirkin, C. A.; Letsinger, R. L.; Mucic, R. C.; Storhoff, J. J., A DNA-based method for rationally assembling nanoparticles into macroscopic materials. *Nature* **1996,** *382* (6592), 607-9.

7. Alivisatos, A. P.; Johnsson, K. P.; Peng, X.; Wilson, T. E.; Loweth, C. J.; Bruchez, M. P., Jr.; Schultz, P. G., Organization of 'nanocrystal molecules' using DNA. *Nature* **1996,** *382* (6592), 609-11.

8. Cutler, J. I.; Auyeung, E.; Mirkin, C. A., Spherical nucleic acids. *J Am Chem Soc* **2012,** *134* (3), 1376-91.

9. Seferos, D. S.; Prigodich, A. E.; Giljohann, D. A.; Patel, P. C.; Mirkin, C. A., Polyvalent DNA nanoparticle conjugates stabilize nucleic acids. *Nano Lett* **2009,** *9* (1), 308-11.

10. Somasuntharam, I.; Yehl, K.; Carroll, S. L.; Maxwell, J. T.; Martinez, M. D.; Che, P. L.; Brown, M. E.; Salaita, K.; Davis, M. E., Knockdown of TNF-alpha by DNAzyme gold nanoparticles as an anti-inflammatory therapy for myocardial infarction. *Biomaterials* **2016,** *83*, 12-22.

11. Mintzer, M. A.; Simanek, E. E., Nonviral vectors for gene delivery. *Chem Rev* **2009,** *109* (2), 259-302.

12. Prigodich, A. E.; Seferos, D. S.; Massich, M. D.; Giljohann, D. A.; Lane, B. C.; Mirkin, C. A., Nano-flares for mRNA regulation and detection. *ACS Nano* **2009,** *3* (8), 2147-52.

13. Halo, T. L.; McMahon, K. M.; Angeloni, N. L.; Xu, Y.; Wang, W.; Chinen, A. B.; Malin, D.; Strekalova, E.; Cryns, V. L.; Cheng, C.; Mirkin, C. A.; Thaxton, C. S., NanoFlares for the detection, isolation, and culture of live tumor cells from human blood. *Proc Natl Acad Sci U S A* **2014,** *111* (48), 17104-9.

14. NU-0129 in Treating Patients With Recurrent Glioblastoma or Gliosarcoma Undergoing Surgery. https://clinicaltrials.gov/ct2/show/NCT03020017?term=SNA&cond=Glioblastoma&rank=1 (accessed March 14, 2019).

15. Kim, D.; Rossi, J., RNAi mechanisms and applications. *Biotechniques* **2008,** *44* (5), 613-6.

16. Service, R. F. Spherical RNA therapy shows promise against psoriasis in first human trial. https://www.sciencemag.org/news/2016/08/spherical-rna-therapy-shows-promise-against-psoriasis-first-human-trial.

17.   Exicure Exicure Announces Top-line Patient Data for Phase 1 Inflammation Program in Psoriasis. http://investors.exicuretx.com/phoenix.zhtml?c=254193&p=irol-newsArticle&ID=2380820.

18.   Rosi, N. L.; Giljohann, D. A.; Thaxton, C. S.; Lytton-Jean, A. K.; Han, M. S.; Mirkin, C. A., Oligonucleotide-modified gold nanoparticles for intracellular gene regulation. *Science* **2006,** *312* (5776), 1027-30.

19.   Case, C. C.; Dhundale, A. R., Gene regulation by antisense RNA and DNA. *Antisense Res Dev* **1991,** *1* (2), 207-17.

20.   Martinovich, K. M.; Shaw, N. C.; Kicic, A.; Schultz, A.; Fletcher, S.; Wilton, S. D.; Stick, S. M., The potential of antisense oligonucleotide therapies for inherited childhood lung diseases. *Mol Cell Pediatr* **2018,** *5* (1), 3.

21.   Breaker, R. R., DNA enzymes. *Nat Biotechnol* **1997,** *15* (5), 427-31.

22.   Silverman, S. K., Deoxyribozymes: DNA catalysts for bioorganic chemistry. *Org Biomol Chem* **2004,** *2* (19), 2701-6.

23.   Yehl, K.; Joshi, J. P.; Greene, B. L.; Dyer, R. B.; Nahta, R.; Salaita, K., Catalytic deoxyribozyme-modified nanoparticles for RNAi-independent gene regulation. *ACS Nano* **2012,** *6* (10), 9150-7.

24.   Petree, J. R.; Yehl, K.; Galior, K.; Glazier, R.; Deal, B.; Salaita, K., Site-Selective RNA Splicing Nanozyme: DNAzyme and RtcB Conjugates on a Gold Nanoparticle. *ACS Chem Biol* **2018,** *13* (1), 215-224.

25.   Zaki, N. M.; Tirelli, N., Gateways for the intracellular access of nanocarriers: a review of receptor-mediated endocytosis mechanisms and of strategies in receptor targeting. *Expert Opin Drug Deliv* **2010,** *7* (8), 895-913.

26.   Vacha, R.; Martinez-Veracoechea, F. J.; Frenkel, D., Receptor-mediated endocytosis of nanoparticles of various shapes. *Nano Lett* **2011,** *11* (12), 5391-5.

27.   Elkin, S. R.; Lakoduk, A. M.; Schmid, S. L., Endocytic pathways and endosomal trafficking: a primer. *Wien Med Wochenschr* **2016,** *166* (7-8), 196-204.

28.   Cooper, G. M., Lysosomes. In *The Cell: A Molecular Approach*, 2nd ed.; Sinauer Associates: Sunderland, 2000.

29.   Choi, C. H.; Hao, L.; Narayan, S. P.; Auyeung, E.; Mirkin, C. A., Mechanism for the endocytosis of spherical nucleic acid nanoparticle conjugates. *Proc Natl Acad Sci U S A* **2013,** *110* (19), 7625-30.

30.   Wu, X. A.; Choi, C. H.; Zhang, C.; Hao, L.; Mirkin, C. A., Intracellular fate of spherical nucleic acid nanoparticle conjugates. *J Am Chem Soc* **2014,** *136* (21), 7726-33.

31.   Mason, D.; Lévy, R., Sticky-flares: real-time tracking of mRNAs... or of endosomes? *BioRxiv* **2015**.

32.   Mason, D.; Carolan, G.; Held, M.; Comenge, J.; Lévy, R., The Spherical Nucleic Acids mRNA Detection Paradox. ResearchGate, 2015.

33.   Lévy, R., Three little (nano) controversies and their morals. 2017.

34.   Czarnek, M.; Bereta, J., SmartFlares fail to reflect their target transcripts levels. *Sci Rep* **2017,** *7* (1), 11682.

35.   Carnevale, K. J. F.; Riskowski, R. A.; Strouse, G. F., A Gold Nanoparticle Bio-Optical Transponder to Dynamically Monitor Intracellular pH. *ACS Nano* **2018**.

36.   Deng, Z. J.; Morton, S. W.; Bonner, D. K.; Gu, L.; Ow, H.; Hammond, P. T., A plug-and-play ratiometric pH-sensing nanoprobe for high-throughput investigation of endosomal escape. *Biomaterials* **2015,** *51*, 250-256.

37.	Zheng, F. F.; Zhang, P. H.; Xi, Y.; Chen, J. J.; Li, L. L.; Zhu, J. J., Aptamer/Graphene Quantum Dots Nanocomposite Capped Fluorescent Mesoporous Silica Nanoparticles for Intracellular Drug Delivery and Real-Time Monitoring of Drug Release. *Anal Chem* **2015,** *87* (23), 11739-45.

38.	Benjaminsen, R. V.; Sun, H.; Henriksen, J. R.; Christensen, N. M.; Almdal, K.; Andresen, T. L., Evaluating nanoparticle sensor design for intracellular pH measurements. *ACS Nano* **2011,** *5* (7), 5864-73.

39.	Kent, K. P.; Childs, W.; Boxer, S. G., Deconstructing green fluorescent protein. *J Am Chem Soc* **2008,** *130* (30), 9664-5.

40.	Phillips, G. J., Green fluorescent protein--a bright idea for the study of bacterial protein localization. *FEMS Microbiol Lett* **2001,** *204* (1), 9-18.

41.	Hink, M. A.; Griep, R. A.; Borst, J. W.; van Hoek, A.; Eppink, M. H.; Schots, A.; Visser, A. J., Structural dynamics of green fluorescent protein alone and fused with a single chain Fv protein. *J Biol Chem* **2000,** *275* (23), 17556-60.

42.	Crone, D. E.; Huang, Y. M.; Pitman, D. J.; Schenkelberg, C.; Fraser, K.; Macari, S.; Bystroff, C., GFP-Based Biosensors. *Intech Open* **2013**.

43.	Magliery, T. J.; Wilson, C. G.; Pan, W.; Mishler, D.; Ghosh, I.; Hamilton, A. D.; Regan, L., Detecting protein-protein interactions with a green fluorescent protein fragment reassembly trap: scope and mechanism. *J Am Chem Soc* **2005,** *127* (1), 146-57.

44.	Shekhawat, S. S.; Ghosh, I., Split-protein systems: beyond binary protein-protein interactions. *Curr Opin Chem Biol* **2011,** *15* (6), 789-97.

45.	De Las Rivas, J.; Fontanillo, C., Protein-protein interactions essentials: key concepts to building and analyzing interactome networks. *PLoS Comput Biol* **2010,** *6* (6), e1000807.

46.	Cabantous, S.; Terwilliger, T. C.; Waldo, G. S., Protein tagging and detection with engineered self-assembling fragments of green fluorescent protein. *Nat Biotechnol* **2005,** *23* (1), 102-7.

47.	Cabantous, S.; Waldo, G. S., In vivo and in vitro protein solubility assays using split GFP. *Nat Methods* **2006,** *3* (10), 845-54.

48.	Lonn, P.; Kacsinta, A. D.; Cui, X. S.; Hamil, A. S.; Kaulich, M.; Gogoi, K.; Dowdy, S. F., Enhancing Endosomal Escape for Intracellular Delivery of Macromolecular Biologic Therapeutics. *Sci Rep* **2016,** *6*, 32301.

49.	Milech, N.; Longville, B. A.; Cunningham, P. T.; Scobie, M. N.; Bogdawa, H. M.; Winslow, S.; Anastasas, M.; Connor, T.; Ong, F.; Stone, S. R.; Kerfoot, M.; Heinrich, T.; Kroeger, K. M.; Tan, Y. F.; Hoffmann, K.; Thomas, W. R.; Watt, P. M.; Hopkins, R. M., GFP-complementation assay to detect functional CPP and protein delivery into living cells. *Sci Rep* **2015,** *5*, 18329.

50.	Kim, J. S.; Choi, D. K.; Park, S. W.; Shin, S. M.; Bae, J.; Kim, D. M.; Yoo, T. H.; Kim, Y. S., Quantitative assessment of cellular uptake and cytosolic access of antibody in living cells by an enhanced split GFP complementation assay. *Biochem Biophys Res Commun* **2015,** *467* (4), 771-7.

51.	Slyusareva, E. A.; Gerasimova, M.; Sizykh, A.; Gornostaev, L. M., Spectral and Fluorescent Indication of the Acid-Base Properties of Biopolymer Solutions. *Russian Physics Journal* **2011,** *54*, 81-87.

52.	pH Indicators. In *The Molecular Probes Handbook*, 11th ed.; Scientific, T., Ed. 2010; p 886.

53.   Hurst, S. J.; Lytton-Jean, A. K.; Mirkin, C. A., Maximizing DNA loading on a range of gold nanoparticle sizes. *Anal Chem* **2006,** *78* (24), 8313-8.

54.   Liang, P.; Canoura, J.; Yu, H.; Alkhamis, O.; Xiao, Y., Dithiothreitol-Regulated Coverage of Oligonucleotide-Modified Gold Nanoparticles To Achieve Optimized Biosensor Performance. *ACS Appl Mater Interfaces* **2018,** *10* (4), 4233-4242.

55.   Akinc, A.; Langer, R., Measuring the pH environment of DNA delivered using nonviral vectors: implications for lysosomal trafficking. *Biotechnol Bioeng* **2002,** *78* (5), 503-8.

56.   Lonn, P.; Dowdy, S. F., Cationic PTD/CPP-mediated macromolecular delivery: charging into the cell. *Expert Opin Drug Deliv* **2015,** *12* (10), 1627-36.

57.   Li, M.; Tao, Y.; Shu, Y.; LaRochelle, J. R.; Steinauer, A.; Thompson, D.; Schepartz, A.; Chen, Z. Y.; Liu, D. R., Discovery and characterization of a peptide that enhances endosomal escape of delivered proteins in vitro and in vivo. *J Am Chem Soc* **2015,** *137* (44), 14084-93.

58.   Zasloff, M., Antimicrobial peptides of multicellular organisms. *Nature* **2002,** *415* (6870), 389-95.

59.   Reinhardt, A.; Neundorf, I., Design and Application of Antimicrobial Peptide Conjugates. *Int J Mol Sci* **2016,** *17* (5).

60.   Rai, D. K.; Qian, S., Interaction of the Antimicrobial Peptide Aurein 1.2 and Charged Lipid Bilayer. *Sci Rep* **2017,** *7* (1), 3719.

61.   Liu, B.; Liu, J., Freezing Directed Construction of Bio/Nano Interfaces: Reagentless Conjugation, Denser Spherical Nucleic Acids, and Better Nanoflares. *J Am Chem Soc* **2017,** *139* (28), 9471-9474.